

Title: Mapping Canopy Damage from Understory Fires in Amazon Forests Using Annual Time Series of Landsat and MODIS Data

Authors: Douglas C. Morton <sup>a,\*</sup>, Ruth S. DeFries <sup>b,c</sup>, Jyoteshwar Nagol <sup>a</sup>, Carlos M. Souza, Jr. <sup>d</sup>, Eric S. Kasischke <sup>a</sup>, George C. Hurtt <sup>e,f</sup>, Ralph Dubayah <sup>a</sup>

<sup>a</sup> Department of Geography, 2181 LeFrak Hall, University of Maryland, College Park, MD 20742 (jnagol@geog.umd.edu, ekasisch@mail.umd.edu, dubayah@umd.edu)

<sup>b</sup> Department of Ecology, Evolution, and Environmental Biology, Columbia University, New York, NY 10027 (rd2402@columbia.edu)

<sup>c</sup> Lamont-Doherty Earth Observatory, Palisades, NY 10964

<sup>d</sup> Instituto do Homem e Meio Ambiente da Amazônia (IMAZON), Belém, Pará, Brazil (souzajr@amazon.org.br)

<sup>e</sup> Institute for the study of Earth, Oceans, and Space (EOS), University of New Hampshire, Durham, NH 03824 (george.hurtt@unh.edu)

<sup>f</sup> Department of Natural Resources, University of New Hampshire, Durham, NH 03824

\* Corresponding Author, Present Address:

Douglas C. Morton  
NASA Goddard Space Flight Center  
Biospheric Sciences Branch  
Code 614.4  
Greenbelt, MD 20771  
Email: douglas.morton@nasa.gov  
Telephone: 301-614-6688  
Fax: 301-614-6695

## Abstract

Understory fires in Amazon forests alter forest structure, species composition, and the likelihood of future disturbance. The annual extent of fire-damaged forest in Amazonia remains uncertain due to difficulties in separating burning from other types of forest damage in satellite data. We developed a new approach, the Burn Damage and Recovery (BDR) algorithm, to identify fire-related canopy damages using spatial and spectral information from multi-year time series of satellite data. The BDR approach identifies understory fires in intact and logged Amazon forests based on the reduction and recovery of live canopy cover in the years following fire damages and the size and shape of individual understory burn scars. The BDR algorithm was applied to time series of Landsat (1997-2004) and MODIS (2000-2005) data covering one Landsat scene (path/row 226/068) in southern Amazonia and the results were compared to field observations, image-derived burn scars, and independent data on selective logging and deforestation. Landsat resolution was essential for detection of burn scars <50 ha, yet these small burns contributed only 12% of all burned forest detected during 1997-2002. MODIS data were suitable for mapping medium (50-500 ha) and large (>500 ha) burn scars that accounted for the majority of all fire-damaged forest in this study. Therefore, moderate resolution satellite data may be suitable to provide estimates of the extent of fire-damaged Amazon forest at a regional scale. In the study region, Landsat-based understory fire damages in 1999 (1508 km<sup>2</sup>) were an order of magnitude higher than during the 1997-1998 El Niño event (124 km<sup>2</sup> and 39 km<sup>2</sup>, respectively), suggesting a different link between climate and understory fires than previously reported for other Amazon regions. The results in this study illustrate the potential to address critical questions concerning climate and fire risk in Amazon forests by applying the BDR algorithm over larger areas and longer image time series.

## 1. Introduction

25

Fire is an important cause of tropical forest degradation with myriad impacts on forest structure, biodiversity, and nutrient cycling (Goldammer 1990; Cochrane 2003). In Amazonia, forest fires occur when human ignitions for deforestation or land management escape their intended boundaries and burn into neighboring forest areas (e.g., Uhl and Buschbacher 1985; Cochrane et al. 1999). Understory forest fires are surface fires that burn leaf litter and coarse woody debris in both logged and intact Amazon forests (Holdsworth and Uhl 1997; Souza et al. 2005a; Balch et al. 2008; Matricardi et al. 2010). Damages from understory fires in tropical forests can be severe, reducing species richness by 30% and above-ground live biomass by up to 50% (Cochrane and Schulze 1999). Even moderate-intensity understory fires can result in high canopy mortality, as few Amazon forest species have fire-adapted traits (Uhl and Kauffman 1990). Widespread forest fires in Amazonia were reported during drought conditions associated with the El Niño Southern Oscillation (ENSO) in 1997-1998 (Barbosa and Fearnside 1999; Elvidge et al. 2001; Phulpin et al. 2002; Alencar et al. 2006), yet the interannual variation in burned forest extent remains uncertain due to difficulties in separating fires from other forest damages using satellite data.

40

Fire, selective logging, and deforestation are related and often sequential forest disturbances in dynamic Amazon frontier landscapes (Uhl and Buschbacher 1985; Nepstad et al. 1999; Alencar et al. 2004; Souza et al. 2005a; Asner et al. 2006; Matricardi et al. 2010). Thus, isolating the unique contribution from fire to forest degradation requires reconciling the spatial and spectral similarities among disturbance types in satellite imagery (Figure 1). Detecting understory forest fires is further complicated by the partial or complete obscuration of actively burning fires and burn damages by intact forest canopies. Previous methods to map understory

45

forest fires in Amazonia have combined field data with high-resolution imagery from a single date to identify canopy damage from fire in near-real time (Elvidge et al. 2001; Phulpin et al. 2002; Brown et al. 2006) or during the subsequent dry season (Pereira and Setzer 1993; 50 Cochrane and Souza 1998; Alencar et al. 2004; Souza et al. 2005a; Matricardi et al. 2010). However, single-date methods are ill-equipped to separate fire-related canopy damage from conventional logging and deforestation that may be spectrally similar in any given year (e.g., Cochrane et al. 1999; Souza et al. 2005a; Souza et al. 2005b). Changes in forest structure remain 55 visible for several years following fire exposure (Cochrane and Souza 1998; Souza et al. 2005b), whereas canopy closure removes evidence of most logging within one year (Asner et al. 2004; Souza et al. 2005b) and deforestation for pasture or cropland remains cleared following forest conversion (Morton et al. 2006), introducing the possibility that a method based on satellite image time series over three or more years may aid the separation of disturbance types in 60 Amazonia.

Time series of satellite imagery have been used to map burned forest at a range of spatial and temporal scales (e.g., Lopez Garcia and Caselles 1991; Kasischke and French 1995; Viedma et al. 1997; Barbosa et al. 1999; Roy et al. 2002; Anderson et al. 2005; Giglio et al. 2009). In most biomes, multiple images within a single season can accurately track the timing and extent 65 of vegetation fires, but approaches based on frequent observations have lower performance in tropical forest regions due to persistent cloud cover and subtle changes in surface reflectance associated with sub-canopy burning (Eva and Lambin 1998; Roy et al. 2008; Giglio et al. 2009), except during drought conditions (Shimabukuro et al. 2009). Evidence of forest disturbance and recovery in time series of annual or biannual Landsat imagery has been used to identify forest 70 fires in northern Spain (Viedma et al. 1997) and logging activity in North America (Kennedy et

al. 2007). Souza *et al.* (2005b) documented a similar trajectory of loss and recovery of green vegetation fraction over four years following fire in an Amazon forest. Building on these efforts, we designed a multi-year, time-series approach to differentiate canopy damage related to understory fires from other forest damages. Throughout the manuscript, we refer to the reduction in live canopy cover from understory forest fires in intact or logged forests as fire-damaged forest. The extent of fire-damage forest may differ from the actual burned area in regions with little or no canopy damage following an understory fire. However, one advantage of our method is that reductions in live canopy cover over large, contiguous areas can be more easily identified using optical remote sensing data than the spectral characteristics of ash or charred vegetation that may be obscured by remaining live canopy trees and understory vegetation following fire in Amazon forests.

This paper describes the development of the Burn Damage and Recovery algorithm (BDR) to map the annual extent of canopy damage from understory fires in Amazonia based on the unique trajectory of disturbance and recovery for fire-damaged forests in time series of dry-season imagery. We applied the BDR algorithm to time series of Landsat and MODIS data to compare the ability to detect forest fire damages in imagery with different spatial resolution. Landsat data (30 m) are an important intermediary between field information and MODIS data because higher-resolution data allow detection of small forest disturbances and visual confirmation of field locations. Advantages of 250 m MODIS data for time series processing and burn detection include reduced data volumes, consistent data quality (e.g., atmospheric correction, accurate geolocation, and data compositing to reduce cloud cover), and more homogenous depiction of canopy damage that may facilitate automated detection approaches and regional-scale studies. The goals of this study were three-fold: 1) to evaluate the accuracy of the

BDR approach for mapping fire-damaged forest using field validation data and independent,  
95 satellite-based estimates of selective logging and deforestation, 2) to determine what size burned  
scars are appropriate for detection with moderate and high-resolution data, and 3) to estimate the  
interannual variability in fire-damaged forest area in ENSO and non-ENSO years during 1997-  
2002 for a study region in southern Amazonia.

## 2. Methods

### 2.1 Study Area

105

We mapped the annual extent of canopy damage from forest fires for a study area (Landsat scene 226/068) in central Mato Grosso state, Brazil (Figure 2). In the past decade, the region experienced high rates of deforestation for cattle ranching and soybean cultivation (Morton et al. 2005; Morton et al. 2006) and forest degradation from selective logging (Asner et al. 2005; Matricardi et al. 2005; Souza et al. 2005b; Matricardi et al. 2007), but the unique contribution from fire to forest degradation has received less attention (Matricardi et al. 2010). The 29,275 km<sup>2</sup> study area was 77% forested in 1997 (>70% shade-normalized green vegetation fraction, following Souza et al., 2005a) and lies predominantly within the Xingu River basin near the southern extent of Amazon forests. Rainfall in the study area is highly seasonal, averaging 1890 mm per year during 1998-2005 with <100 mm per month during May-September based on data from the Tropical Rainfall Measuring Mission (TRMM 3B343, Huffman et al. 2007). Prior to analysis, topographic data (SEPLAN-MT 2004) were used to exclude 1,450 km<sup>2</sup> of water and seasonally-inundated vegetation for three main tributaries of the Xingu River (Rio Manissuiá-Miçu, Rio Arraias, and Rio Ferro) in order to avoid spurious errors associated with interannual changes in river levels or unreliable vegetation index values over water (Figure 2).

120

### 2.2 Satellite-Based Measures of Fire Effects in Amazon Forests

Canopy damage from understory fires in Amazon forests is highly variable. Field studies suggest that understory fires may kill 6-44% of trees >10 cm diameter at breast height, and canopy mortality is typically higher in logged forests than in undisturbed forests (Holdsworth and Uhl 1997; Barbosa and Fearnside 1999; Pinard et al. 1999; Barlow et al. 2003; Haugaasen et

125

al. 2003; Ivanauskas et al. 2003; Balch et al. 2008). Canopy mortality from understory fire also exhibits fine-scale spatial heterogeneity (see Figure 1). Edaphic conditions and differential mortality among tree species may partially explain these patterns (Ivanauskas et al. 2003),  
130 although the distribution of leaf litter and fine fuels may also be important for patterns of understory burning and related canopy mortality in more seasonal Amazon forests (Balch et al. 2008).

In the months following fire, the patchy distribution of high and low canopy damage areas from understory fires can be detected with high-resolution optical remote sensing data  
135 (e.g., Figure 1, Cochrane and Souza 1998; Souza and Roberts 2005). Optical remote sensing data are sensitive to changes in live canopy cover, consistent with field measurements of canopy damages from understory fires. In the first year following fire, Haugaasen et al. (2003) reported an increase in canopy gap fraction from 5% to 19%, and Balch et al. (2008) measured a 16% decline in LAI. Over longer time scales, delayed mortality of large trees three or more years  
140 following fire has important consequences for net carbon storage in Amazon forests (Barlow et al. 2003). However, changes in surface reflectance from delayed mortality of large trees are likely to be offset by a reduction in canopy gap fraction from growth of remaining trees and recruitment of new individuals in the years following fire damages (Barlow and Peres 2008).

We derived two parameters of canopy damage from fire using high and moderate  
145 resolution satellite data. Because the BDR algorithm uses imagery from the early dry season to detect evidence of burning from the previous year, this study mapped post-fire effects on canopy trees and not burned area, *per se* (Lentile et al. 2006). Therefore, we refer to canopy damage from understory fires as fire-damaged forest area rather than burned area. The total fire-damaged forest area was calculated as the sum of all pixels within the study area with canopy

150 damage from fire. Individual burn scars of different sizes were delineated from the map of fire-  
damaged forest area based on contiguous patches of canopy damage. Given the fine-scale spatial  
heterogeneity in canopy damage from fire observed in field and satellite-based studies, burn  
scars derived from both high and moderate resolution satellite data may include some fraction of  
unburned forest within individual burn scars, while burned forest areas that do not exhibit  
155 canopy damage may be excluded.

## 2.3 Data

We used a variety of data sources to build and test the BDR algorithm for mapping the  
extent of canopy damage from fire. Below, we describe the pre-processing steps to generate dry-  
160 season time series of Landsat and MODIS data and the satellite and field data used to calibrate  
the BDR algorithm. Section 2.4 provides a detailed description of the BDR algorithm. Finally,  
Section 2.5 presents the approach for validation of the satellite-based maps of canopy damage  
from fire using field observations of burned forest, image-derived validation data, and  
independent data products on selective logging and deforestation.

### 165 2.3.1 Landsat TM 1997-2004

We used a time series of annual Landsat TM/ETM+ data (Table 1) for the Mato Grosso  
study area to characterize patterns of disturbance and recovery from fire at high resolution (30  
m). Image preprocessing, including georegistration and atmospheric correction, was described in  
170 detail by Souza et al. (2005a). Briefly, reflectance values in annual dry-season Landsat images  
from June-August of each year (1997-2004) were normalized to one atmospherically-corrected  
scene (1999), and a linear spectral mixture model with common endmembers for green  
vegetation (GV), non-photosynthetic vegetation (NPV), shade, and soil was used to derive

annual fraction images and normalized difference fraction index (NDFI) data layers (Souza et al. 2005a; Souza et al. 2005b). Images were co-registered to the 1999 ETM+ reference scene, with root mean square (RMS) error <1 pixel in all years (Souza et al. 2005a; Souza et al. 2005b). In this study, we analyzed annual shade-normalized green vegetation fraction (GVs) data layers from 1997-2004 following the calculation presented by Souza *et al.*, (2005a):

$$GV_s = \frac{GV}{(100 - Shade)} \quad (1)$$

Souza *et al.* (2005a) showed that the GV fraction was best for separating logged and burned forests, while the composite NDFI was best for separating logged and intact forest classes:

$$NDFI = \frac{GV_s - (NPV + Soil)}{GV_s + (NPV + Soil)} \quad (2)$$

### 2.3.2 MODIS 250 m Dry-season Mean NDVI 2000-2005

We constructed an annual time series of MODIS dry-season mean normalized difference vegetation index (mNDVI) to detect evidence of forest disturbance and recovery from fire at moderate resolution (250 m). mNDVI data layers were produced by averaging dry-season NDVI values from the Collection 4 MOD13 Q1 Vegetation Indices (Huete et al. 2002). The MOD13 product is based on atmospherically-corrected surface reflectance data (Vermote et al. 2002), and MODIS has sub-pixel geolocation accuracy (Wolfe et al. 2002). Annual mNDVI data values for each 250 m pixel were derived from seven 16-day composite periods (day of year 129, 145, 161, 177, 193, 209, and 225) in order to 1) limit interference from clouds or biomass burning aerosols typical of wet-season and late dry-season months, respectively, 2) eliminate artifacts from new forest burning that occurs during the late dry season, and 3) maintain consistent solar illumination conditions relative to the June solstice to minimize the impacts of seasonal changes

in solar illumination on canopy reflectance. Remaining cloudy or other low-quality data values identified in the Quality Assurance data layer were replaced using a local spline function based on remaining high-quality data values in each pixel's time series (Morton et al. 2006) prior to averaging for each annual mNDVI data layer for 2000-2005. Finally, in order to evaluate evidence of fire damage in 2000 MODIS data from fires in 1999, all regions were assigned a forested mNDVI value in 1999 (mNDVI = 0.85). Landsat-based results for fire-damaged forest during 1998 and 1999 were used to quantify the fraction of historic burning from these years that was visible in 2000 MODIS imagery.

### 205        2.3.3 Calibration Data

We used existing satellite-based data products and field observations to assess the spatial and temporal patterns of forest disturbances in time series of Landsat and MODIS data (Table 2). Forest damages that occurred between 2002 and 2003 were selected for algorithm calibration based on overlap with the MODIS era. Calibration data for both logged forest and logged forests that subsequently burned were identified using results from Souza et al. (2005a) and were visually inspected to eliminate areas that were later deforested using data from the PRODES (Monitoramento da Floresta Amazônica Brasileira por Satélite) annual Landsat-based deforestation assessments (INPE 2007). Field observations of intact forest in July 2005 were used to identify forest areas that were not logged, burned, or cleared during the combined Landsat and MODIS time series (1997-2005). Finally, deforestation events >25 ha with post-clearing land use of either pasture or cropland were selected to compare time series trajectories among major classes of forest cover change within the study area (Morton et al. 2006; INPE 2007). Calibration data totaled approximately 100 km<sup>2</sup> for each class (Table 2).

Calibration data were used to assess the separability of fire damages from other unburned  
220 cover types based on the trajectory of GVs and mNDVI over time (Figure 3, Table 3). Similar  
vegetation greenness among forest disturbance classes in individual years highlights the value of  
a time series approach for isolating canopy damages from fire in Amazonia (Figure 3).  
For example, in 2003, the range of mNDVI and GVs for burned forest was similar to logged  
forest and deforestation for pasture. However, the multi-year trajectory of burn damage and  
225 recovery is unique (Figure 3). Calibration data on burned forest were used to set the transition  
rules for the trajectory of burn damage and recovery in the BDR algorithm (Table 3). In a per-  
pixel analysis, the BDR trajectory excluded >99.8% of calibration data for intact forest, logged  
forest, and deforestation for cropland in time series of Landsat and MODIS data (Table 4). A  
small fraction of calibration data for pasture deforestation exhibited the BDR trajectory at  
230 Landsat (1.8%) or MODIS resolution (4.2%). The BDR algorithm also uses spatial attributes  
(size, shape) and spectral characteristics (mean greenness) of fire-damaged forest areas to isolate  
understory forest fires from other cover types, based on calibration data at Landsat and MODIS  
resolutions.

#### 235 2.4 Burn Damage and Recovery (BDR) Algorithm

The BDR algorithm is a time-series approach to distinguish fire-related canopy damage  
from selective logging and deforestation (Figure 4). The BDR algorithm is comprised of three  
main processing components: Trajectory Analysis, Contextual Analysis, and Attribute Analysis.  
During Trajectory Analysis, a moving 4-year window is used to compare each pixel's time series  
240 of Landsat or MODIS observations to the BDR trajectory to identify core areas of canopy  
damage from fire each year. The BDR time series trajectory for fire-damaged forest (Figure 3,

Table 3) is comprised of: 1) forested conditions in the year prior to burning, 2) intermediate change in post-burn vegetation greenness, relative to either logging or deforestation (0.75 years post-fire), and 3) recovery of mNDVI or GVs values during subsequent years (1.75 and 2.75 years post-fire). Clusters of neighboring pixels that satisfy all criteria for pre-burn, post-burn, and recovery elements of the BDR trajectory and exceed the minimum size criteria are considered core areas (Figure 4). To minimize confusion between canopy damage from fire and selective logging, the BDR algorithm only identifies core areas at Landsat resolution that are four times larger (1.5 ha) than previously reported for log landing areas in selective logging operations (0.4 ha) (Souza et al. 2005a). At MODIS resolution, the minimum core area is 10 ha. Compared to single image classification or image differencing techniques, the BDR approach provides 3+ observations to confirm the trajectory of burn damage and forest recovery. We note that the BDR algorithm identifies fire-damaged forests on a one year delay because at least one year of forest recovery is required to confirm understory fire damages rather than deforestation for agricultural use (see Figure 3).

The second component of the BDR algorithm is Contextual Analysis. During Contextual Analysis, core burned areas are grown into larger regions using a neighborhood search for adjacent pixels that meet BDR trajectory criteria for growth regions (Table 4, Figure 4). Compared to core areas of canopy damage from fire, pixels that fit the growth region BDR trajectory have a wider range of pre-burn, post-burn, and recovery values, consistent with mixed pixels of burned forest with other cover types (Figure 4). Growth regions must be adjacent to core areas to be included in the BDR algorithm. A similar, two-phase classification approach was used previously to map burned forest in Alaska with AVHRR data (Kasischke and French 1995).

265           The final component of the BDR algorithm, Attribute Analysis, analyzes the spatial and spectral characteristics of each burn scar (Figure 4). Spatial and spectral statistics include the size, perimeter-area ratio, average greenness in the year of burn detection, and interior fraction. Interior fraction was selected as a better measure of burn scar shape for MODIS results than perimeter-area ratio, calculated based on the reduction in burn scar size after applying a majority  
270 filter to the initial results using a 3 x 3 pixel window. These spatial and spectral statistics form the basis of a burn scar confidence classification, developed based on algorithm calibration data (see Table 2), in which large, non-linear burn scars with low average post-burn greenness are considered most confident. Low confidence burn scars at Landsat resolution have high perimeter-area ratio typical of the linear or dendritic pattern of selective logging operations;  
275 MODIS low-confidence detections are small or linear features common along class boundaries at moderate resolution (Figure 5). Figure 5 also shows how Landsat and MODIS data provide complimentary information. Low-confidence burn scars at 30 m and 250 m resolutions rarely overlap, whereas high confidence burn scars at Landsat and MODIS resolutions are largely coincident. The final outputs of the BDR algorithm are annual maps of fire-damaged forest in  
280 which each burn scar is classified as high or low confidence according to spatial and spectral metrics.

          In summary, the BDR algorithm uses the temporal and spatial patterns of canopy damage from fire to isolate burn damages from undisturbed forest, logged forest, and deforested areas. The BDR algorithm applied to time series of Landsat GVs data searches for core areas of  
285 contiguous canopy damage from fire that are at least four times larger than previously documented for log landings in selective logging operations, uses recovery in years 1-2 after damage to differentiate forest burning from deforestation, and analyzes the resulting burn scars

to eliminate overlap with selectively logged forests based on the shape (perimeter-area ratio) and degree of canopy damage within each burn scar (mean GVs). The minimum burn scar size in  
290 Landsat-based results is 1.5 ha, equivalent to the smallest core area considered by the algorithm.

The BDR algorithm applied to time series of MODIS mNDVI also begins with large core areas to search for canopy damage from fire ( $\geq 10.7$  ha). The algorithm excludes single pixel clusters to eliminate potential classification errors from small deforestation or fire events that cannot be well-characterized using moderate resolution data (Morton et al. 2005). MODIS  
295 results are then classified according to confidence levels by size, shape, and mean mNDVI in the year of burn detection. High confidence burn scars are large ( $>50$  ha), non-linear (interior fraction  $>0.6$ ), with intermediate post-burn mNDVI values between logged ( $>0.8$ ) and deforested areas ( $<0.71$ ), and recovery of mNDVI in years 1-2 after canopy damages.

## 300 2.5 Validation

We evaluated the accuracies of burn scars from the BDR algorithm using four independent validation datasets and an inter-comparison of high-confidence Landsat and MODIS results (Table 2). Figure 6 summarizes the overall approach for analysis and validation of results from the BDR algorithm. Omission and commission were calculated on a per-pixel and per-  
305 polygon basis. Per-pixel comparisons quantified the total overlap between validation data and fire-damaged forest. Per-polygon analyses quantified the overlap between BDR results and validation data for individual validation polygons (perimeters) of different sizes. We stratified omission and commission errors by polygon size to quantify the advantages and disadvantages of the BDR algorithm applied to high and moderate resolution time series. The accuracies of both  
310 low and high-confidence detections were evaluated in order to 1) test whether spatial and

spectral metrics derived from calibration data reduced the overlap with independent estimates of logging and deforestation, and 2) evaluate the potential for MODIS to identify small burn scars. Each validation dataset is briefly described below.

Field observations of forests that burned in 1999-2002 were collected during June-  
315 September of 2001 and 2003 (DCM, RSD). In each year, field transects along existing roads targeted fire scars visible in coincident high-resolution imagery. The location and perimeter of each forest burn scar was recorded using a hand-held Global Positioning System (GPS) unit. The date and ignition source for each fire was determined using a combination of satellite data and information from landowners. Immediately following field campaigns, field-mapped burn  
320 perimeters were identified in coincident high-resolution data (ASTER or Landsat TM/ETM+) to complete portions of the burn perimeter that were not accessible during fieldwork. The total fire-damaged forest area mapped during fieldwork was 145 km<sup>2</sup> in 18 forest burn scars that ranged in size from 27-5,086 ha (Table 5).

We generated an additional validation dataset of burned forest perimeters from 1999  
325 through visual inspection of Landsat imagery from 1999-2001. Spatial and spectral characteristics of field-mapped forest burn scars were used to identify similar features within the study area. A total of 145 forest burn scars from 1999 (1767.9 km<sup>2</sup>), ranging in size from 13-14,462 ha, were digitized within the study area to test omission of canopy damage from fire in the BDR results (Figure 7). For per-polygon analyses, we used linear regression to determine  
330 whether the area of fire-damaged forest identified in Landsat and MODIS results within individual validation burn scars was similar for burn scars of different sizes. We ran separate regression analyses for large (>500 ha) and small/medium (<500 ha) burn scars.

Agreement between fire-damaged forest results from Landsat and MODIS time series was used as an additional validation test since canopy damages are captured differently in high and moderate resolution data (see Figure 5). Subtle damages from selective logging are less likely to be detected with moderate resolution data than with data from Landsat-like sensors (Asner et al. 2004), while mixed pixel effects at class boundaries typical at MODIS resolution are less likely to occur with higher resolution data (Morton et al. 2005). Therefore, detection by both MODIS and Landsat BDR results increases the confidence of an individual burn scar. To compare the burn scar results from moderate and high resolution data, linear regression was used to determine whether the area identified in Landsat results (y) was similar to the area identified in MODIS results (x). Separate regression analyses were run for large (>500 ha) and small/medium (<500 ha) burn scars. We also calculated the fraction of the total fire-damaged forest in high-confidence burn scars that was detected at both Landsat and MODIS resolutions each year.

Independent datasets on selective logging (Asner et al. 2005) and deforestation (INPE 2007) were used to characterize potential commission errors in the Landsat and MODIS-based results of fire-damaged forest. These comparisons did not provide a rigorous test of commission errors in results from the BDR algorithm because neither logging nor deforestation data products were specifically designed to exclude burned forest. Instead, evaluation of overlap between canopy damage from fire, selective logging, and deforestation was useful to characterize the nature and extent of classification confusion among disturbance types in southern Amazonia. Overlap between deforestation events >25 ha and fire-damaged forests was further evaluated according to post-clearing land use based on results from Morton *et al.* (2006). Finally, accounting methods differ between the BDR algorithm and datasets of selective logging and

deforestation. For fire-damaged forest, images from the early dry season capture evidence of forest burning during the previous dry season. Selective logging and deforestation damages were assigned to the year in which they were mapped, representing the sum of all damages between annual images. For validation, this study compared fire-damaged forests, selective logging, and deforestation identified in the same year (e.g., burn damages from 1999 were compared with selective logging from 2000 since both were derived from 2000 Landsat data, burn damages from 2002 were compared with 2003 deforestation, etc.). For consistency, this study described validation comparisons using the year of burn damages.

365

### 3.Results

#### 3.1 Validation: Omission

Field and image-derived forest burn scars were used to quantify omission in results from  
370 the BDR algorithm applied to Landsat and MODIS time series. Overall, the BDR algorithm  
accurately identified forest burn scars mapped during fieldwork (Table 5). Landsat results  
identified some canopy damage from fire in all 18 field-mapped burn scars, and MODIS results  
detected fire damages in all but one field-mapped burn scar in 2000 (size = 103 ha). MODIS  
results more closely matched burn perimeters mapped during fieldwork than Landsat results due  
375 to heterogeneity of canopy damage within the burn scar that truncated the Contextual Analysis  
component of the BDR algorithm at Landsat resolution. All of the field-mapped burn scars were  
identified as high-confidence results at Landsat and MODIS resolutions (Table 5).

Landsat and MODIS-based results for fire-damaged forest in 1999 identified burn  
damages in 99% and 94% of image-derived burn scars, respectively (Table 5). Landsat results  
380 detected 61% of the total fire-damaged forest area (pixels within the burn perimeter), with some  
canopy damage from fire detected in 143/145 burn scars. The fraction of digitized burn scars  
detected by Landsat was consistent for large (>500 ha,  $y = 0.63x$ ,  $R^2 = 0.96$ ,  $n = 65$ ) and small  
validation burn scars (<500ha,  $y = 0.68x$ ,  $R^2 = 0.97$ ,  $n = 81$ , Figure 8a). MODIS results detected  
a higher percentage of the total fire-damaged forest area (76%) but fewer individual burn scars  
385 than Landsat (136/145). Four of the 9 digitized forest burn scars without a corresponding  
MODIS detection were <50 ha. Results from MODIS underestimated the area within the  
perimeter of individual burn scars by approximately 25% for digitized burn scars of all sizes  
(>500 ha,  $y = 0.75x$ ,  $R^2 = 0.97$ ,  $n = 65$ ; <500 ha,  $y = 0.74x$ ,  $R^2 = 0.89$ ,  $n = 81$ , Figure 7b). Nearly  
all 1999 burn scars were characterized as high-confidence results at both Landsat and MODIS

390 resolutions; large burn scars (>500 ha) accounted for 93% of the total digitized area (see Figure  
7).

### 3.2 Validation: Commission

#### 3.2.1 Selective Logging

395 Independent maps of annual selective logging damages (Asner et al. 2005) were used to  
characterize potential commission errors in results from the BDR algorithm. Overlap between  
selective logging and canopy damage from fire was high in 1999 but very low in 2000 and 2001  
(Table 6). Coincident burning and logging classifications in 1999 were predominantly in high-  
confidence results (Table 6). Forest areas classified as logged and burned in 1999 also  
400 overlapped with 52% of field-mapped burn scars and 48% of digitized forest burn scars in that  
year. In 2000 and 2001, there was little overlap between fire-damaged forest and selective  
logging, and most coincident detections occurred in the low-confidence burn scars. In all years,  
forest burning extended beyond the area identified as both logged and burned. For example,  
burn scars in Landsat and MODIS results from 1999 that were also classified as logging  
405 averaged only 49% and 33% logged, respectively.

#### 3.2.2 Deforestation

Landsat-based maps of annual deforestation from the PRODES program (INPE 2007)  
were also used to quantify potential commission errors in results from the BDR algorithm.  
410 Overlap between fire-damaged forest and PRODES deforestation occurred primarily in high-  
confidence burn scars (Table 7). The area of overlap between fire-damaged forest and  
deforestation was similar for Landsat and MODIS results in all years (Table 7).

Coincident detection of burn damages and deforestation varied according to clearing size and post-clearing land use (Table 7). In 2000 and 2001, confusion between deforestation and fire-damaged forest was mostly confined to large (>25 ha) forest clearings for pasture. Burn scars only overlapped with a small fraction of the individual areas cleared for pasture in those years; the average fraction of forest clearings for pasture mapped as canopy damage from fire was 28% in 2000 and 25% in 2001. In 2002, a small number of individual clearings for pasture (37/192) that were mapped as >50% fire-damaged forest accounted for 75% of the area of overlap between deforestation for pasture and fire-damaged forest in that year. Forest burn scars overlapped less frequently with deforestation classified as not in agricultural production (NIP), and did not overlap with cropland deforestation and clearings <25 ha except in 2002 (Table 7).

### 3.3 Interannual Variation in Fire-Damaged Forest, 1997-2002

The majority of fire-damaged forest mapped with Landsat and MODIS time series was not associated with the 1997-1998 ENSO. Fire-damaged forest area in 1999 was 10 and 15 times greater than the amount of canopy damage from fire identified during 1997 and 1998, respectively (Table 8). Similarly, nearly all of the burning attributed to 1999 in the analysis of MODIS data from 2000 was unrelated to the ENSO event; less than 1% of MODIS fire-damaged forest area in 1999 was classified as burned during 1998 in Landsat-based results (12 km<sup>2</sup>). Due to rapid recovery of canopy greenness following fire, imagery from the first year following understory fire damages is critical to identify and follow the fate of burned Amazon forests.

Interannual variation in fire-damaged forest area was similar between results from the BDR algorithm applied to Landsat and MODIS time series (Table 8). The location of individual burn scars during 1999-2002 was also similar between moderate and high-resolution results.

MODIS burn scars with corresponding Landsat detections accounted for over 91% of all MODIS high confidence fire-damaged forest area (Table 8).

In the southern Amazon study area, the total Landsat high confidence fire-damaged forest area during 1997-2002 was 2136 km<sup>2</sup> (Table 6), equivalent to 10% of all forest in the study area in 1997 (Figure 9). The total area in high confidence burn scars during 1999-2002 at MODIS resolution was 2832 km<sup>2</sup> (13% of 1997 forested area).

### 3.4 Burn Scar Sizes

The contribution of large and small burn scars to total fire-damaged forest area varied interannually (Figure 10). Large burn scars (>500 ha) were only identified in years with highest fire damages (1999, 2002). However, these largest burn scars contributed the majority of canopy damage from fire during 1997-2002. Burn scars >500 ha accounted for 56% of the Landsat fire-damaged forest area during 1997-2002 and 78% of the MODIS fire-damaged forest area during 1999-2002.

Small burn scars (<50 ha) in Landsat results were common in all years but contributed only 12% of the total fire-damaged forest area over the study period. Small burn scars contributed 46% of total fire-damaged forest area in years with lowest canopy damage from fire (1998, 2001).

The estimated size of individual burn scars was larger from MODIS than from Landsat, but the exact relationship between MODIS and Landsat-based area was strongly dependent on burn scar size. For large burn scars (>500 ha), MODIS-based burn scar size (x) was consistently twice that derived from Landsat data (y): 1999 ( $y = 0.52x$ ,  $R^2 = 0.92$ ,  $n = 79$ ) and 2002 ( $y = 0.49x$ ,  $R^2 = 0.94$ ,  $n = 19$ ) (Figure 11). The correlation between MODIS and Landsat-based burn scar size was lower for smaller burn scars (<500 ha), and the slope of the linear fit was more

460 variable (1999:  $y = 0.23x$ ,  $R^2 = 0.47$ ,  $n = 200$ ; 2000:  $y = 0.40x$ ,  $R^2 = 0.82$ ,  $n = 38$ ; 2001:  $y = 0.23x$ ,  $R^2 = 0.56$ ,  $n = 30$ ; and 2002:  $y = 0.37x$ ,  $R^2 = 0.68$ ,  $n = 105$ . Data not shown).

#### 4. Discussion

465           The BDR algorithm is a novel approach to estimate the annual extent of canopy damage from understory fires in Amazon forests. The use of satellite image time series and spatial attributes of burn scars enabled accurate identification of fire-damaged forest areas and improved separability of burning from logging and deforestation compared to single-date methods. Results from the BDR algorithm applied to time series of Landsat and MODIS data demonstrate the high  
470 degree of interannual variability in the extent of fire-damaged forest. Unexpectedly, fire-damaged forest in 1999 was an order of magnitude higher than during the 1997-1998 El Niño. Large burn scars (>500 ha) were also detected in 2002, highlighting potential differences in the relationship between climate and fire in this study area compared to Amazon regions with highest fire damages reported during ENSO-related drought events (e.g., Barbosa and Fearnside  
475 1999; Nepstad et al. 2004; Alencar et al. 2006). Our results illustrate the potential to address critical questions concerning climate and fire risk in Amazon forests when the BDR algorithm is applied over larger areas.

##### 4.1 Fire-damaged forest in southern Amazonia

480           Interannual variation in fire-damaged forest area was high within the study area in southern Amazonia. Fires damaged 10% of all forest in the study area during 1997-2002, and three quarters of all canopy damage from fire occurred during 1999. Findings in this study were similar to results from Matricardi et al. (2010) for burn damages in 1999. In contrast, Alencar et al. (2006) reported extensive fire damages in 1998 for a neighboring study area in northern Mato  
485 Grosso state, Brazil. At least three factors could contribute to regional differences in understory fire damages in southern Amazonia. First, high rates of selective logging in our study area

(Asner et al. 2005; Souza et al. 2005a; Matricardi et al. 2007; Matricardi et al. 2010) may have increased the risk of understory forest fires (Uhl and Buschbacher 1985; Holdsworth and Uhl 1997; Nepstad et al. 1999). Second, differences in climate and soils may contribute to the  
490 observed interannual differences in understory forest fire damages in the region. Although the network of meteorological stations in Amazonia is sparse, merged precipitation products from gauge measurements and satellite sensors (Huffman et al. 2007) offer the possibility to evaluate regional climate patterns preceding and during widespread understory fire activity identified using the BDR approach. Third, drought conditions in Amazonia are associated with increased  
495 rates of tree mortality (Brando et al. 2007). It is therefore possible that drought-induced tree mortality from the 1997-1998 ENSO event increased understory fire risk in later years. The potential for these differences in land use, climate, or forest structure to generate spatial heterogeneity in understory forest fire damages in Amazonia merits further study.

Very large burn scars were only identified during years with extensive forest burning,  
500 consistent with previous findings of greater penetration of understory fires in periodic high-fire years (Cochrane and Laurence 2002; Alencar et al. 2004; Alencar et al. 2006). Based on understory fire spread rates of 0.1 – 0.5 m/min (Cochrane et al. 1999; Balch et al. 2008), the largest fires in 1999 may have burned continuously for approximately two weeks. Whether high fire damages in these years were linked with climate (Ray et al. 2005) or an increase in fuel  
505 availability (Holdsworth and Uhl 1997; Alvarado et al. 2004; Balch et al. 2008), prolonged rainless periods once understory fires begin appear necessary for individual fires to damage large areas.

Once burned, Amazon forests may be more susceptible to future fires based on the influence of canopy damage on forest microclimate and fuels (Cochrane et al. 1999). By

510 extending the length of the satellite data time series, the BDR approach could also be used to  
characterize the frequency of fires in previously-burned forest to evaluate long-term changes in  
the structure of tropical forest ecosystems from frequent fire exposure (Cochrane and Schulze  
1999; Barlow and Peres 2008).

## 515 4.2 BDR Approach

MODIS and Landsat data time series have complementary characteristics for mapping  
canopy damage from fire in tropical forests. Lower data volumes and a more homogenous  
disturbance signature in 250 m MODIS data facilitated BDR processing; some canopy damage  
was not detected at Landsat resolution because damaged pixels were not contiguous, interrupting  
520 the neighborhood search in the Contextual Analysis component of the BDR algorithm.  
Therefore, MODIS results more closely matched validation burn perimeters than Landsat results.  
Landsat data were essential for detecting small burn scars (<50 ha) and fire damages prior to the  
MODIS era. Landsat-based results also suggested that only half of the forest area within large  
burn perimeters exhibited canopy damage, similar to field studies of canopy mortality from fire  
525 in Amazonia. Advantages of Landsat resolution for evaluating the patterns and severity of  
canopy mortality within the burn perimeter, as identified in previous field studies (e.g., Cochrane  
and Schulze 1999; Haugaasen et al. 2003; Balch et al. 2008), are an important area for future  
study. Given the tradeoffs in spatial resolution between MODIS and Landsat, a multi-satellite  
approach may be most efficient for targeting high-resolution analyses of fire damages based on  
530 initial burn perimeters mapped with moderate resolution data.

The BDR approach successfully isolated fire-damaged forest from areas of selective  
logging in years with low fire activity such as 2001, when <0.4% of logging was classified as

burning and <9% of burning was also classified as logging. Given previous reports of low sensitivity to fine-scale canopy damages from selective logging in moderate resolution data (e.g.,  
535 Asner et al. 2004), the high degree of confusion between MODIS-based burn scars and logging in 1999 was unexpected (821 km<sup>2</sup> represented 31% of logging and 33% of canopy damage from fire). Overlap between validation burn scars and selective logging suggests that logging and burning may have occurred in the same year (1999) or that burning re-exposed evidence of selective logging prior to 1999. Clarifying the role of logging for generating both fuels and  
540 ignition sources for forest fires in Amazonia during years with extensive forest fire damages is an important subject for future study.

Overlap between deforestation and fire-damaged forest in both Landsat and MODIS results suggests that PRODES may have overestimated the amount of deforestation in the study area in 2002. In 2000 and 2001, overlap between deforestation and burning classifications  
545 represented <5% of total deforested area, whereas coincident deforestation and burning detection in 2002 (108-115 km<sup>2</sup>) was approximately 17% of total deforestation that year. Because the BDR algorithm identifies areas of fire-damaged forest based on forest recovery over time, it is likely that the areas of overlap between burn scars and deforestation were never fully cleared for agricultural use. Our results further suggest that cropland expansion may be a more important  
550 driver of recent deforestation than previously reported (Morton et al. 2006) because most overlap between forest burning and PRODES deforestation was associated with clearing for pasture. Lower overlap between mechanized forest clearing for cropland and fire-damaged forest may be a result of seasonal differences in the timing of fires for deforestation; fires for cropland deforestation occur earlier in the dry season than fires for pasture deforestation when  
555 surrounding forests may be less flammable (Morton et al. 2008). However, confusion between

forest fires and deforestation cannot be completely resolved by combining independent data products derived from different methods (image differencing and time-series approaches).

Development of an integrated time-series approach to separately account for the contributions from understory fires, selective logging, and deforestation to annual forest damage would satisfy information needs for both policy and science applications. All three types of forest disturbance could be identified in time series of data from Landsat-like sensors by combining methods demonstrated in this study to follow fire damages and deforestation over time with techniques to detect spatial attributes of forestry infrastructure (Asner et al. 2005; Matricardi et al. 2005; Souza et al. 2005a). Time series of MODIS data could be used to estimate fire-damaged forest and deforestation in an internally-consistent manner, given that MODIS-based results in this study were largely insensitive to subtle canopy damages from selective logging. Any integrated approach that requires several years of satellite imagery will not replace the need for operational deforestation monitoring (INPE, 2006) or global burn scar mapping (e.g., Roy et al. 2008; Giglio et al. 2009). As presented here, the BDR algorithm can only map canopy damages from fire with high confidence on a two-year delay in order to track both canopy damage and recovery. However, longer time horizons under discussion for policy and market mechanisms for Reducing Emissions from Deforestation and forest Degradation, conservation and enhancement of forest carbon stocks, and sustainable forest management (REDD+) may permit this type of retrospective approach (Gullison et al. 2007), given the substantial differences in forest carbon losses from understory fires (e.g., Barlow et al. 2003; Alencar et al. 2006; Balch et al. 2008), selective logging (e.g., Keller et al. 2004; Huang et al. 2008), and deforestation (Houghton et al. 2000; van der Werf et al. 2009).

### 4.3 Uncertainties

580 Validation efforts in this study provide a rigorous test of the BDR algorithm based on the best available data. Omission of fire-damaged forest was tested using field and image-derived validation burn scars, and commission errors were evaluated using independent data on selective logging and deforestation in the region. However, no “gold standard” reference information on understory fire extent was available to resolve uncertainties when independent data products on  
585 forest disturbance overlapped or to test omission and commission errors at a regional scale. The time series approach presented here, in combination with field observations or very high resolution (<5m) remote sensing data, can help resolve whether overlap among existing products represents misclassification or sequential forest disturbances. Reducing uncertainties in the rates of deforestation and forest degradation remains a priority in Amazonia and other tropical forest  
590 regions, especially given burgeoning international efforts for REDD+.

Several limitations of the BDR algorithm may lead to an underestimate of fire-damaged forest in this study. The BDR algorithm may not detect understory fires that do not generate any canopy damage or forests that burn every year. Similarly, fires that generate very low or very high canopy damage may be considered low confidence detections to minimize potential  
595 classification errors with selective logging and deforestation, respectively. Good correspondence between field observations of burned forest and BDR results suggests that canopy recovery following fire is characteristic of burning events in the study region. However, burned forests that do not recover in years following fire damages will be underestimated by the BDR algorithm. Future work in this area is needed to characterize the levels of canopy damage from  
600 fire identified by the BDR approach, including the impacts of repeated fires on burn detection. During sequential forest disturbance events, such as fire following selective logging (Souza et al.

2005a), fire damages that follow the network of skid roads and log decks installed during forestry operations may not be considered high confidence burn scars in the BDR approach. Finally, immediate abandonment of partially-cleared areas or installation of plantation forests  
605 could generate a recovery trajectory similar to burned forest, leading to commission errors with the BDR approach. Data on land abandonment and plantation forests were not available, but based on field knowledge of the study region these practices are rare relative to widespread damages from understory fires, selective logging, and deforestation for agricultural use.

610 5. Conclusions

The BDR algorithm is a novel method to identify spatial and temporal characteristics of burned forest in time series of satellite data. Time series of annual dry season data from a minimum of three consecutive years permits detection of two changes—a reduction in green vegetation following fire and immediate recovery of canopy material in subsequent years. The results from this study demonstrate that both Landsat and MODIS time series are suitable for isolating understory forest fire damages from selective logging and deforestation in Amazonia using the BDR algorithm. Although MODIS-based results more closely matched validation burn perimeters, complementary information from MODIS and Landsat resolution time series suggest that a combined approach may be useful to characterize the extent and severity of canopy damage from understory fires in Amazonia, respectively.

Mapping the annual extent of canopy damage from understory fires in Amazonia is critical to improve estimates of carbon emissions from forest degradation to meet both scientific and policy objectives. This study confirmed that periodic high fire years contribute substantially to forest degradation in southern Amazonia. However, the two years with most extensive burning in the study area (1999, 2002) did not coincide with the 1997-1998 ENSO as reported in previous studies. Large fires (>500 ha) were only detected in 1999 and 2002, indicating that climatic conditions in these years may have allowed slow-moving understory fires to burn continuously for several weeks. Applying the BDR algorithm to longer time series and larger study areas will improve understanding of relationships among climate, land use, and forest fire activity in Amazonia. In particular, the BDR approach offers the possibility to assess interannual variability in understory forest fire damages for tropical forest regions that experience a range of seasonal and interannual precipitation patterns.

## 6. Acknowledgements

This work was supported by the NASA Large-scale Biosphere-Atmosphere Experiment in Amazonia (LBA-ECO) and Land-Cover and Land-Use Change Programs (LCLUC). Support for D. Morton was also provided under the NASA Earth and Space Science Fellowship (ESSF) and NASA Postdoctoral Program (NPP). Data on selective logging were graciously provided by Greg Asner and David Knapp. The authors thank Ane Alencar, Liana Anderson, Matthew Hansen, Marcelo Latorre, Ellen Jasinski, Britaldo Soares-Filho, and Yosio Shimabukuro for their support and assistance with field data collection. In addition, we thank Louis Giglio and Wilfrid Schroeder for productive discussions on fire and fire mapping related to the BDR approach presented in this manuscript.

## References

- Alencar, A., Nepstad, D.C., & Vera Diaz, M.d.C. (2006). Forest understory fire in the Brazilian Amazon in ENSO and non-ENSO years: Area burned and committed carbon emissions. *Earth Interactions*, *10*, Paper 10-006.
- Alencar, A., Solórzano, L.A., & Nepstad, D.C. (2004). Modeling forest understory fires in an eastern Amazonian landscape. *Ecological Applications*, *14*, S129-S149.
- Alvarado, E.C., Sandberg, D.V., Carvalho Jr., J.A., Gielow, R., & Santos, J.C. (2004). Landscape fragmentation and fire vulnerability in the primary forest adjacent to recent land clearings in the Amazon arc of deforestation. *Floresta*, *34*, 169-174.
- Anderson, L.O., Aragao, L.E., Lima, A., & Shimabukuro, Y.E. (2005). Detecção de cicatrizes de áreas queimadas baseada no modelo linear de mistura espectral e imagens índice de vegetação utilizando dados multitemporais do sensor MODIS/TERRA no estado do Mato Grosso, Amazônia brasileira. *Acta Amazonica*, *35*, 445-456.
- Asner, G.P., Broadbent, E.N., Oliveira, P.J.C., Keller, M., Knapp, D.E., & Silva, J.N. (2006). Condition and fate of logged forests in the Brazilian Amazon. *Proceedings of the National Academy of Sciences*, *103*, 12947-12950.
- Asner, G.P., Keller, M., Pereira, R., Zweede, J.C., & Silva, J.N. (2004). Canopy damage and recovery following selective logging in an Amazon forest: Integrating field and satellite studies. *Ecological Applications*, *14*, 280-298.
- Asner, G.P., Knapp, D.E., Broadbent, E.N., Oliveira, P.J.C., Keller, M., & Silva, J.N. (2005). Selective logging in the Brazilian Amazon. *Science*, *310*, 480-482.
- Balch, J.K., Nepstad, D.C., Brando, P.M., Curran, L.M., Portela, O., de Carvalho Jr., O., & Lefebvre, P. (2008). A negative fire feedback in a transitional forest of southeastern Amazonia. *Global Change Biology*, *14*, 1-12.
- Barbosa, P.M., Grégoire, J.-M., & Pereira, J.M.C. (1999). An algorithm for extracting burned areas from time series of AVHRR GAC data applied at a continental scale. *Remote Sensing of Environment*, *69*, 253-263.
- Barbosa, R.I., & Fearnside, P.M. (1999). Incêndios na Amazônia Brasileira: Estimativa da emissão de gases do efeito estufa pela queima de diferentes ecossistemas de Roraima na passagem do evento "El Niño" (1997/1998). *Acta Amazonica*, *29*, 513-534.
- Barlow, J., & Peres, C.A. (2008). Fire-mediated dieback and compositional cascade in an Amazonian forest. *Philosophical Transactions of the Royal Society of London B*, *363*, 1787-1794.
- Barlow, J., Peres, C.A., Lagan, B., & Haugaasen, T. (2003). Large tree mortality and the decline of forest biomass following Amazonian wildfires. *Ecology Letters*, *6*, 6-8.
- Brando, P.M., Nepstad, D.C., Davidson, E.A., Trumbore, S.E., Ray, D., & Camargo, P. (2007). Drought effects on litterfall, wood production and belowground carbon cycling in an Amazon forest: results of a throughfall reduction experiment. *Philosophical Transactions of the Royal Society of London B*, doi:10.1098/rstb.2007.0031.
- Brown, I.F., Schroeder, W., Setzer, A.W., Maldonado, M.L.R., Pantoja, N., Duarte, A., & Marengo, J. (2006). Monitoring fires in southwestern Amazonia rain forests. *Eos Transactions of the American Geophysical Union*, *87*, 253.
- Cochrane, M., Alencar, A., Schulze, M., Souza Jr., C.M., Nepstad, D.C., Lefebvre, P., & Davidson, E.A. (1999). Positive feedbacks in the fire dynamic of closed canopy tropical forests. *Science*, *284*, 1832-1835.
- Cochrane, M.A. (2003). Fire science for rainforests. *Nature*, *421*, 913-919.

- Cochrane, M.A., & Laurence, W.F. (2002). Fire as a large-scale edge effect in Amazonian forests. *Journal of Tropical Ecology*, 18, 311-325.
- Cochrane, M.A., & Schulze, M.D. (1999). Fire as a recurrent event in tropical forests of the eastern Amazon: effects on forest structure, biomass, and species composition. *Biotropica*, 31, 2-16.
- Cochrane, M.A., & Souza, C.M. (1998). Linear mixture model classification of burned forests in the eastern Amazon. *International Journal of Remote Sensing*, 19, 3433-3440.
- Elvidge, C., Hobson, V., Baugh, K., Dietz, J., Shimabukuro, Y.E., Krug, T., Novo, E., & Echavarría, F. (2001). DMSP-OLS estimation of tropical forest area impacted by surface fires in Roraima, Brazil: 1995 versus 1998. *International Journal of Remote Sensing*, 22, 2661-2673.
- Eva, H.D., & Lambin, E.F. (1998). Remote sensing of biomass burning in tropical regions: sampling issues and multisensor approach. *Remote Sensing of Environment*, 64, 292-315.
- Giglio, L., Loboda, T., Roy, D.P., Quayle, B., & Justice, C.O. (2009). An active-fire based burned area mapping algorithm for the MODIS sensor. *Remote Sensing of Environment*, 113, 408-420.
- Goldammer, J.G. (1990). *Fire in the tropical biota: ecosystem processes and global challenges*. New York: Springer-Verlag.
- Gullison, R.E., Frumhoff, P.C., Canadell, J.G., Field, C.B., Nepstad, D.C., Hayhoe, K., Avissar, R., Curran, L.M., Friedlingstein, P., Jones, C., & Nobre, C.A. (2007). Tropical forests and climate policy. *Science*, 316, 985-986.
- Haugaasen, T., Barlow, J., & Peres, C.A. (2003). Surface wildfires in central Amazonia: short-term impact on forest structure and carbon loss. *Forest Ecology and Management*, 179, 321-331.
- Holdsworth, A.R., & Uhl, C. (1997). Fire in Amazonian selectively logged rain forest and the potential for fire reduction. *Ecological Applications*, 7, 713-725.
- Houghton, R.A., Skole, D.L., Nobre, C.A., Hackler, J.L., Lawrence, K.T., & Chomentowski, W.H. (2000). Annual Fluxes of carbon from deforestation and regrowth in the Brazilian Amazon. *Nature*, 403, 301-304.
- Huang, M., Asner, G.P., Keller, M., & Berry, J.A. (2008). An ecosystem model for tropical forest disturbance and selective logging. *Journal of Geophysical Research*, 113, G01002, doi:10.1029/2007JG000438.
- Huete, A.R., Didan, K., Miura, T., Rodriguez, E.P., Gao, X., & Ferreira, L.G. (2002). Overview of the radiometric and biophysical performance of the MODIS vegetation indices. *Remote Sensing of Environment*, 83, 195-213.
- Huffman, G.J., Adler, R.F., Bolvin, D.T., Gu, G., Nelkin, E.J., Bowman, K.P., Hong, Y., Stocker, E.F., & Wolff, D.B. (2007). The TRMM Multisatellite Precipitation Analysis (TMPA): Quasi-global, multiyear, combined-sensor precipitation estimates at fine scales. *Journal of Hydrometeorology*, 8, 38-55.
- INPE (2007). Projeto PRODES: Monitoramento da floresta Amazônica Brasileira por satélite. In: Instituto Nacional de Pesquisas Espaciais.
- Ivanauskas, N.M., Monteiro, R., & Rodrigues, R.R. (2003). Alterations following a fire in a forest community of Alto Rio Xingu. *Forest Ecology and Management*, 184, 239-250.
- Kasischke, E.S., & French, N. (1995). Locating and estimating the areal extent of wildfires in Alaskan boreal forests using multiple-season AVHRR NDVI composite data. *Remote Sensing of Environment*, 51, 263-275.

- Keller, M., Asner, G.P., Silva, N., & Palace, M. (2004). Sustainability of selective logging of upland forests in the Brazilian Amazon: Carbon budgets and remote sensing as tools for evaluating logging effects. In D.J. Zarin, J.R.R. Alavalapati, F. Putz & M. Schmink (Eds.), *Working Forests in the Neotropics* (pp. 41-63). New York: Columbia.
- Kennedy, R.E., Cohen, W.B., & Schroeder, T.A. (2007). Trajectory-based change detection for automated characterization of forest disturbance dynamics. *Remote Sensing of Environment*, *110*, 370-386.
- Lentile, L.B., Holden, Z.A., Smith, A.M.S., Falkowski, M.J., Hudak, A.T., Morgan, P., Lewis, S.A., Gessler, P.E., & Benson, N.C. (2006). Remote sensing techniques to assess active fire characteristics and post-fire effects. *International Journal of Wildland Fire*, *15*, 319-345.
- Lopez Garcia, M.J., & Caselles, V. (1991). Mapping burns and natural reforestation using Thematic Mapper data. *Geocarto International*, *1*, 31-37.
- Matricardi, E.A.T., Skole, D.L., Cochrane, M., Qi, J., & Chomentowski, W.H. (2005). Monitoring selective logging in tropical evergreen forests using Landsat: multitemporal regional analyses in Mato Grosso, Brazil. *Earth Interactions*, *9*, 1-24.
- Matricardi, E.A.T., Skole, D.L., Cochrane, M.A., Pedlowski, M.A., & Chomentowski, W. (2007). Multi-temporal assessment of selective logging in the Brazilian Amazon using Landsat data. *International Journal of Remote Sensing*, *28*, 63-82.
- Matricardi, E.A.T., Skole, D.L., Pedlowski, M.A., Chomentowski, W., & Fernandes, L.C. (2010). Assessment of tropical forest degradation by selective logging and fire using Landsat imagery. *Remote Sensing of Environment*, *114*, 1117-1129.
- Morton, D.C., DeFries, R.S., Randerson, J.T., Giglio, L., Schroeder, W., & Van der Werf, G.R. (2008). Agricultural intensification increases deforestation fire activity in Amazonia. *Global Change Biology*, *14*, 2262-2275.
- Morton, D.C., DeFries, R.S., Shimabukuro, Y.E., Anderson, L.O., Arai, E., Espirito-Santo, F.d.B., Freitas, R., & Morissette, J. (2006). Cropland expansion changes deforestation dynamics in the southern Brazilian Amazon. *Proceedings of the National Academy of Sciences*, *103*, 14637-14641.
- Morton, D.C., DeFries, R.S., Shimabukuro, Y.E., Anderson, L.O., del bon Espirito-Santo, F., Hansen, M.C., & Carroll, M. (2005). Rapid assessment of annual deforestation in the Brazilian Amazon using MODIS data. *Earth Interactions*, *9*, 22.
- Nepstad, D.C., Lefebvre, P., da Silva, U.L., Tomasella, J., Schlesinger, P., Solórzano, L.A., Moutinho, P., Ray, D., & Benito, J.G. (2004). Amazon drought and its implications for forest flammability and tree growth: a basin-wide analysis. *Global Change Biology*, *10*, 704-717.
- Nepstad, D.C., Veríssimo, A., Alencar, A., Nobre, C.A., Lima, E., Lefebvre, P., Schlesinger, P., Potter, C., Moutinho, P., Mendoza, E., Cochrane, M., & Brooks, V. (1999). Large-scale impoverishment of Amazonian forests by logging and fire. *Nature*, *398*, 505-508.
- Pereira, M.C., & Setzer, A.W. (1993). Spectral characteristics of fire scars in Landsat-5 TM images of Amazonia. *International Journal of Remote Sensing*, *14*, 2061-2078.
- Phulpin, T., Lavenu, F., Bellan, M.F., Mougnot, B., & Blasco, F. (2002). Using SPOT-4 HRVIR and VEGETATION sensors to assess impact of tropical forest fires in Roraima, Brazil. *International Journal of Remote Sensing*, *23*, 1943-1966.
- Pinard, M., Putz, F., & Licona, J. (1999). Tree mortality and vine proliferation following a wildfire in a subhumid tropical forest in eastern Bolivia. *Forest Ecology and Management*, *116*, 247-252.

- Ray, D., Nepstad, D.C., & Moutinho, P. (2005). Micrometeorological and canopy controls on fire susceptibility in a forested landscape. *Ecological Applications*, *15*, 1664-1678.
- Roy, D.P., Boschetti, L., Justice, C.O., & Ju, J. (2008). The collection 5 MODIS burned area product--Global evaluation by comparison with the MODIS active fire product. *Remote Sensing of Environment*, *112*, 3690-3707.
- Roy, D.P., Lewis, P., & Justice, C.O. (2002). Burned area mapping using multi-temporal moderate spatial resolution data--a bi-directional reflectance model-based expectation approach. *Remote Sensing of Environment*, *83*, 263-286.
- SEPLAN-MT (2004). Mapa: Zoneamento Sócio Econômico Ecológico do Estado de Mato Grosso - 2002. GIS data layers for social, economic, and ecological characteristics of Mato Grosso state, Brazil, available at: <http://www.zsee.seplan.mt.gov.br/>. In
- Shimabukuro, Y.E., Duarte, V., Arai, E., Freitas, R.M., Lima, A., Valeriano, D.M., Brown, I.F., & Maldonado, M.L.R. (2009). Fraction images derived from Terra MODIS data for mapping burnt areas in Brazilian Amazonia. *International Journal of Remote Sensing*, *30*, 1537-1546.
- Souza, C.M., & Roberts, D.A. (2005). Mapping forest degradation in the Amazon region with Ikonos images. *International Journal of Remote Sensing*, *26*, 425-429.
- Souza, C.M., Roberts, D.A., & Cochrane, M.A. (2005a). Combining spectral and spatial information to map canopy damage from selective logging and forest fires. *Remote Sensing of Environment*, *98*, 329-343.
- Souza, C.M., Roberts, D.A., & Monteiro, A. (2005b). Multitemporal analysis of degraded forests in the southern Brazilian Amazon. *Earth Interactions*, *9*
- Uhl, C., & Buschbacher, R. (1985). A disturbing synergism between cattle ranch burning practices and selective tree harvesting in the eastern Amazon. *Biotropica*, *17*, 265-268.
- Uhl, C., & Kauffman, J.B. (1990). Deforestation, fire susceptibility, and potential tree responses to fire in the eastern Amazon. *Ecology*, *71*, 437-449.
- van der Werf, G.R., Morton, D.C., DeFries, R.S., Giglio, L., Randerson, J.T., Collatz, G.J., & Kasibhatla, P.S. (2009). Estimates of fire emissions from an active deforestation region in the southern Amazon based on satellite data and biogeochemical modelling. *Biogeosciences*, *6*, 235-249.
- Vermote, E.F., El Saleous, N.Z., & Justice, C.O. (2002). Atmospheric correction of visible to middle infrared EOS-MODIS data over land surface: background, operational algorithm and validation. *Remote Sensing of Environment*, *83*, 97-111.
- Viedma, O., Meliá, J., Segarra, D., & García-Haro, J. (1997). Modeling rates of ecosystem recovery after fires by using Landsat TM data. *Remote Sensing of Environment*, *61*, 383-398.
- Wolfe, R., Nishihama, M., Fleig, A.J., Kuyper, J.A., Roy, D.P., Storey, J.C., & Patt, F.S. (2002). Achieving sub-pixel geolocation accuracy in support of MODIS land science. *Remote Sensing of Environment*, *83*, 31-49.

Table 1. Day of year for annual Landsat (scene 226/068) and MODIS 16-day composite data (tile H12V10) in this study.

Year	Landsat		MODIS
	Day of Year	Sensor	Day of Year
1997	217	TM5	-
1998	157	TM5	-
1999	231	ETM+	-
2000	178	TM5	129-225
2001	220	ETM+	129-225
2002	191	ETM+	129-225
2003	218	TM5	129-225
2004	157	TM5	129-225
2005	-	-	129-225

Table 2. Data sources for calibration and validation of fire-damaged forest area derived from the BDR algorithm.

Class	Calibration			Validation		
	Source	Year*	Area (km <sup>2</sup> )	Source	Year*	Area (km <sup>2</sup> )
Forest	Field Observations	2005	101.6	NA		
Selective Logging	Souza <i>et al.</i> 2005a	2002	102.8	Asner <i>et al.</i> , 2005	1999-2001	5932.3
Burned Forest**	Souza <i>et al.</i> 2005a	2002	105.2	Field Observations; Image-derived burn scars; Landsat/MODIS Inter-comparison	1999-2002; 1999; 1999-2002	144.7; 1767.9; ***
Deforestation****	INPE, 2007; Morton <i>et al.</i> , 2006	2002	Pasture: 89.6; Cropland: 91.6	INPE, 2007; Morton <i>et al.</i> , 2006	2000-2002	1332.6

\* Deforestation and selective logging between annual images are assigned to the end image date by INPE (2007) and Asner *et al.* (2005), respectively. Fire-damaged forest areas are assigned to the beginning date, since early dry-season imagery (May-June) captures evidence of burning from the previous dry season (August-September). For consistency, we report all comparisons according to the year of forest burning from the BDR approach (e.g., Year 1999 = 1999 fire damages and 2000 selective logging).

\*\* Souza *et al.* (2005a) identified forest areas that were logged and subsequently burned. Field and image-derived forest burn scars used for validation were not necessarily logged prior to burning.

\*\*\* Inter-comparison of annual high confidence fire-damaged forest area, total: Landsat (1879.8 km<sup>2</sup>), MODIS (3040.1 km<sup>2</sup>).

\*\*\*\* A subset of INPE PRODES deforestation for 2002, classified according to post-clearing land use as pasture or cropland, was used for BDR calibration. Validation efforts considered all deforestation during 2000-2002 (excluding the calibration subset), classified as cropland, pasture, or not in production (Morton *et al.*, 2006).

Table 3. BDR trajectory parameters for core and growth areas in dry-season imagery for pre and post-burn periods. Limits for the BDR burn trajectories are depicted in Figure 3, with years 1-4 corresponding to the annual intervals described below.

	<b>1. Pre-Burn minimum</b>	<b>Drop (2-1) minimum</b>	<b>2. Post-burn range</b>	<b>3. Recovery (1) minimum</b>	<b>4. Recovery (2) minimum</b>
<b>MODIS mNDVI (0-1)</b>					
Core	0.8	-0.05	0.7-0.8	+0.02	
Growth	0.75	-0.01	0.65-0.83	+0.01	+0.01
<b>Landsat GVs (0-100)</b>					
Core	75	-11	50-70	+6	
Growth	70	-6	35-75	+5	+1

Table 4: Fraction of calibration data for the BDR algorithm classified as a core burned area at MODIS and Landsat resolution.

<b>Class</b>	<b>Area (km<sup>2</sup>)</b>	<b>Landsat Core Burned Area (%)</b>	<b>MODIS Core Burned Area (%)</b>
Forest	101.6	0	0
Logged Forest	102.8	0.05	0.07
Burned Forest	105.2	16.3	33.8
Pasture Deforestation	89.6	1.8	4.2
Cropland Deforestation	91.6	0.02	0.2

Table 5. Detection of field and image-derived validation forest burn scars with results from the BDR algorithm applied to time series of Landsat and MODIS data. Results are presented by area (km<sup>2</sup>) and percent of total validation area detected. The number of observations (obs.) and validation burn scar sizes are also shown for each year.

Year	Obs.	Validation Burn Scars (ha)	Area (km <sup>2</sup> )	Landsat		MODIS		
				km <sup>2</sup>	%	km <sup>2</sup>	%	
<b>Field</b>								
1999	9	34, 205, 237, 496, 505, 820, 1148, 1479, 5086	96.3	78.9	82	82.8	86	
2000*	2	49, 103	1.5	0.8	53	0.3	20	
2001	1	979	9.8	1.1	12	2.5	25	
2002	6	27, 272, 300, 632, 873, 1672	37.2	26.4	71	33.4	90	
Total	18		144.7	107.2	74	119.0	82	
<b>Image</b>								
1999**	145	(see Fig. 6)	1767.9	1071.1	61	1344.5	76	

\* Only year in which results for high-confidence burn scars differed from total (low + high confidence) fire-damaged forest area (Landsat 0.6 km<sup>2</sup>, MODIS = 0).

\*\* Overlap of high confidence burn scars with image-derived validation data differed by <1% from total results (Landsat 1063 km<sup>2</sup>, MODIS 1331 km<sup>2</sup>).

Table 6. Overlap between Landsat-based selective logging from Asner *et al.* (2005) and fire-damaged forest for all BDR results (Total) and high-confidence burn scars (HC) from Landsat and MODIS time series. Total high confidence fire-damaged forest area (HC Area) and the percentage of HC Area that overlapped with selective logging are also shown.

Year*	Logged Area (km <sup>2</sup> )	Landsat HC Area (km <sup>2</sup> )	Landsat Overlap			MODIS HC Area (km <sup>2</sup> )	MODIS Overlap		
			Total (km <sup>2</sup> )	HC (km <sup>2</sup> )	%		Total (km <sup>2</sup> )	HC (km <sup>2</sup> )	%
1999	2587.6	1508.1	653.8	633.4	42	2526.3	848.2	821.0	33
2000	1466.1	55.4	10.7	5.2	9	65.5	12.8	4.4	7
2001	1878.6	34.9	2.2	2.0	6	45.5	11.5	2.8	6

\* Asner *et al.* (2005) assigned logging between annual Landsat images to the end image date, whereas burn damages from the BDR algorithm are attributed to previous year. As shown, year 1999 corresponds to logging in 2000, etc.

Table 7. Overlap between fire-damaged forest (2000-2002) and PRODES deforestation (2001-2003) (INPE, 2007) for all BDR results (Total) and high-confidence burn scars (HC). Total overlap with PRODES deforestation is further divided by size and post-clearing land use (Morton *et al.*, 2006). Total high confidence fire-damaged forest area (HC Area) and the percentage of HC Area that overlapped with deforestation are also shown.

Year*		Deforested Area (km <sup>2</sup> )**	Landsat HC Area (km <sup>2</sup> )	Landsat Overlap			MODIS HC Area (km <sup>2</sup> )	MODIS Overlap		
				Total (km <sup>2</sup> )	HC (km <sup>2</sup> )	%		Total (km <sup>2</sup> )	HC (km <sup>2</sup> )	%
<b>2000</b>	<b>Total</b>	<b>287.0</b>	<b>55.4</b>	<b>13.0</b>	<b>12.9</b>	<b>23</b>	<b>65.5</b>	<b>21.5</b>	<b>11.9</b>	<b>18</b>
	>25 ha									
	Cropland	78.5		0.0	0.0			0.6	0.1	
	Pasture	165.4		10.0	10.0			15.7	8.4	
	NIP	15.3		2.2	2.1			3.7	3.0	
	<25 ha	27.8		0.8	0.8			1.5	0.5	
<b>2001</b>	<b>Total</b>	<b>398.3</b>	<b>34.9</b>	<b>19.3</b>	<b>19.1</b>	<b>55</b>	<b>45.5</b>	<b>26.3</b>	<b>18.7</b>	<b>41</b>
	>25 ha									
	Cropland	113.5		0.0	0.0			0.9	0.0	
	Pasture	225.9		16.1	16.0			18.2	12.5	
	NIP	24.3		2.7	2.6			6.2	5.7	
	<25 ha	34.6		0.5	0.5			1.0	0.5	
<b>2002</b>	<b>Total</b>	<b>649.3</b>	<b>281.4</b>	<b>119.3</b>	<b>115.3</b>	<b>41</b>	<b>402.7</b>	<b>125.6</b>	<b>108.3</b>	<b>27</b>
	>25 ha									
	Cropland	235.2		13.5	13.5			4.3	1.9	
	Pasture	275.2		63.7	63.1			61.5	53.4	
	NIP	75.2		35.3	32.1			49.7	44.2	
	<25 ha	63.7		6.9	6.6			10.2	8.8	

\*Burn year 2000 corresponds to 2001 deforestation due to differences in annual accounting between BDR and PRODES.

\*\*Landsat-based annual deforestation from PRODES (INPE, 2007). Clearings >25 ha classified according to post-clearing land use (Morton *et al.*, 2006).

Table 8. Fire-damaged forest area detected by the BDR algorithm using Landsat and MODIS time series for all forest burn scars (Total) and high-confidence burn scars (HC). Coincident detections at both high and moderate resolution (overlap) were derived from high-confidence burn scars.

<b>Year</b>	<b>Total Fire-damaged Forest Area (km<sup>2</sup>)</b>	<b>HC Fire-damaged Forest Area (km<sup>2</sup>)</b>	<b>Overlap (km<sup>2</sup>)*</b>
<b>Landsat</b>			
1997	150.3	123.6	
1998	41.6	38.6	
1999	1549.9	1508.1	1435.8
2000	67.5	55.4	28.1
2001	35.9	34.9	17.4
2002	290.5	281.4	185.6
<b>MODIS</b>			
1999	2788.7	2526.3	2317.3
2000	143.4	65.5	52.4
2001	88.9	45.5	40.4
2002	507.8	402.7	359.5

\* Forest burn scars with high-confidence detections in Landsat and MODIS results during 1999-2002.

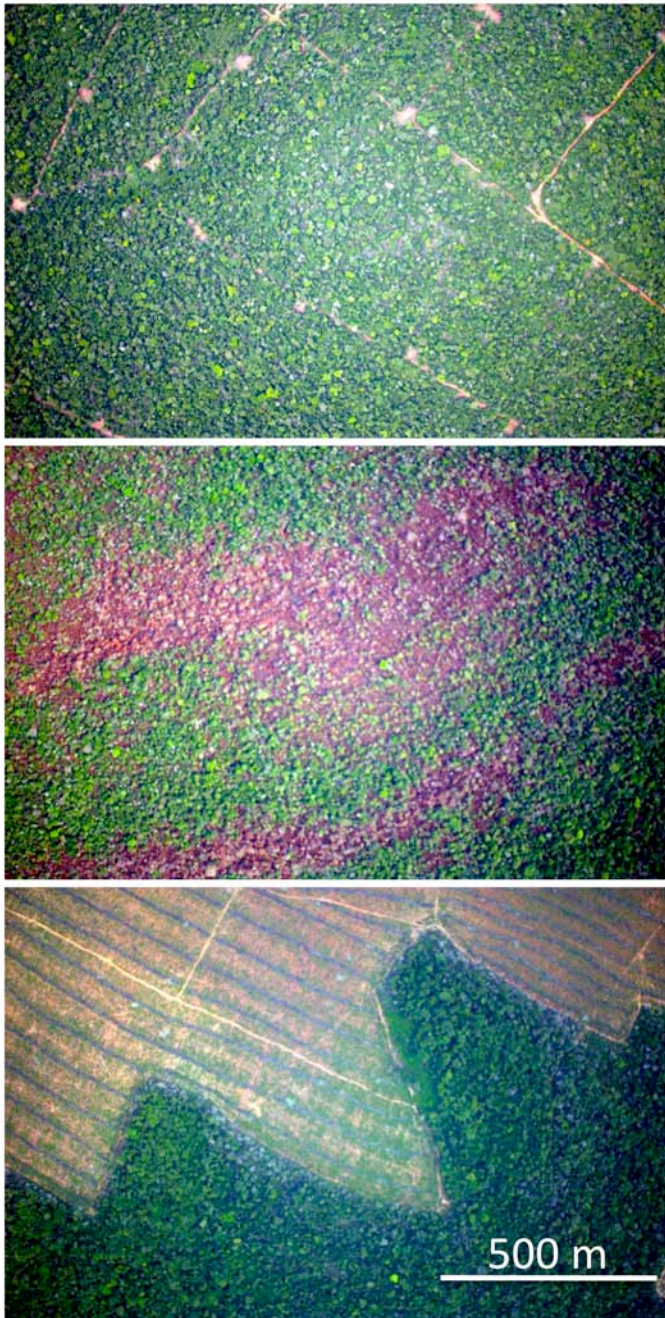


Figure 1. Aerial photographs from the Mato Grosso study region depicting canopy damage from roads and log landing areas (patios) for selective logging (top), understory forest fires (middle), and deforestation for agricultural use (bottom) in 2007. Photo credit: Alberto Setzer, Instituto Nacional de Pesquisas Espaciais (INPE), São José dos Campos, SP, Brazil.

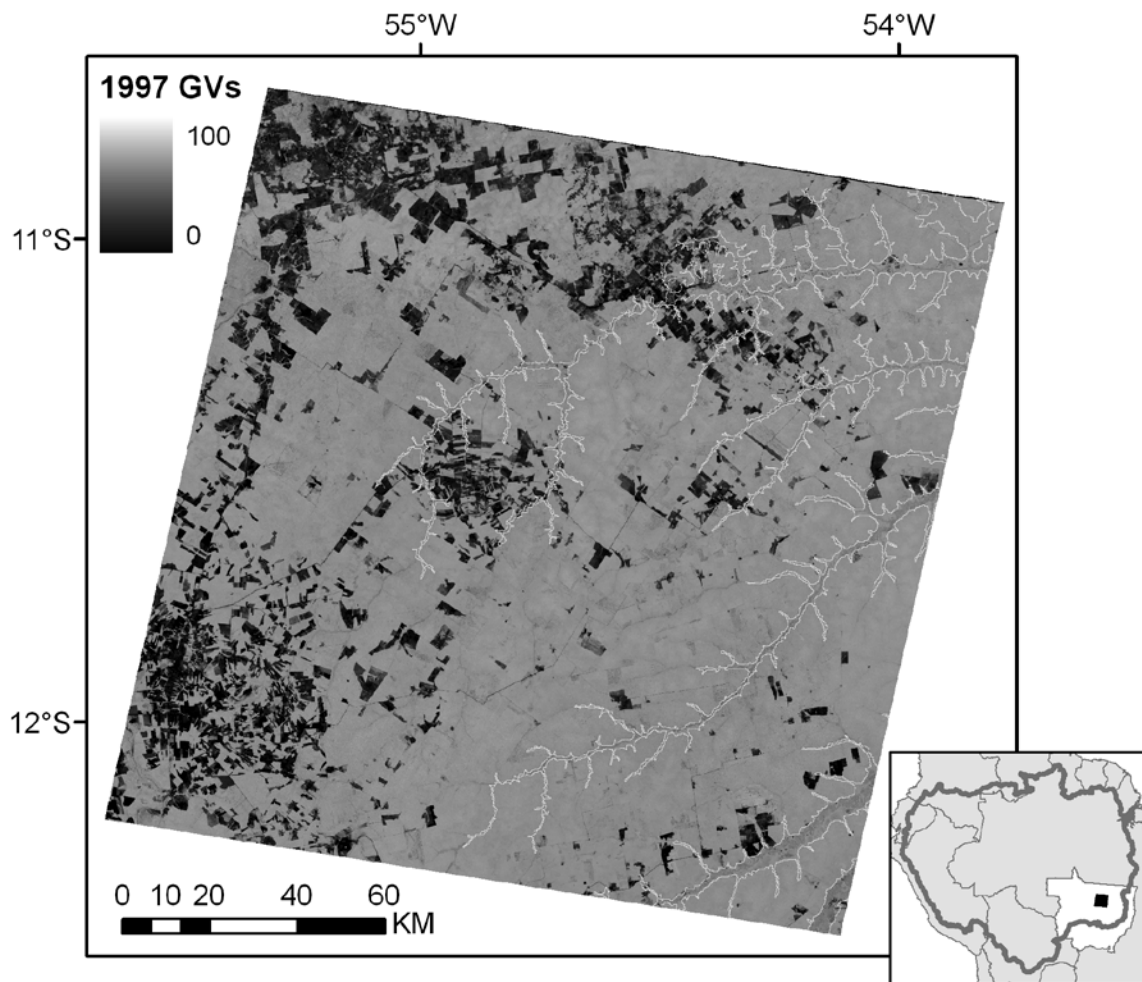


Figure 2: Landsat 1997 shade-normalized green vegetation (GVs) for the study region. Forested regions appear dark gray and deforested regions appear black in this early dry season image. Tributaries of the Xingu River that were excluded from the analysis are outlined in white. Inset: the Landsat study area (black) in central Mato Grosso state (white) lies near the eastern extent of the Amazon Basin (gray outline).

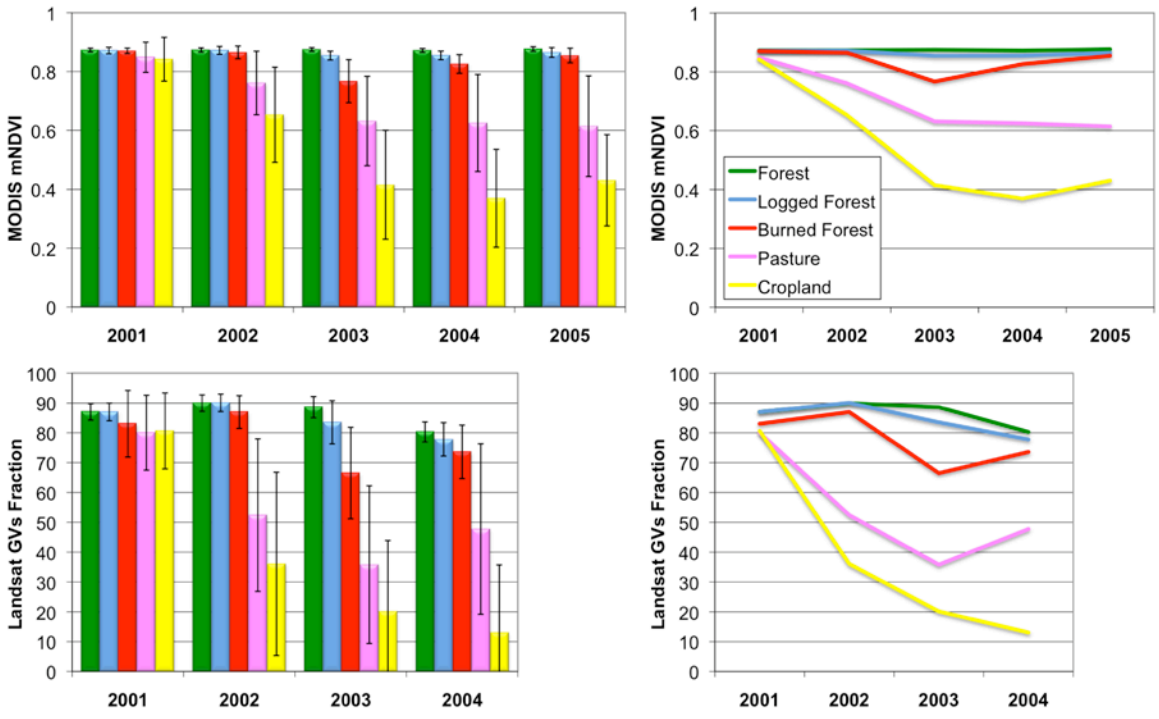
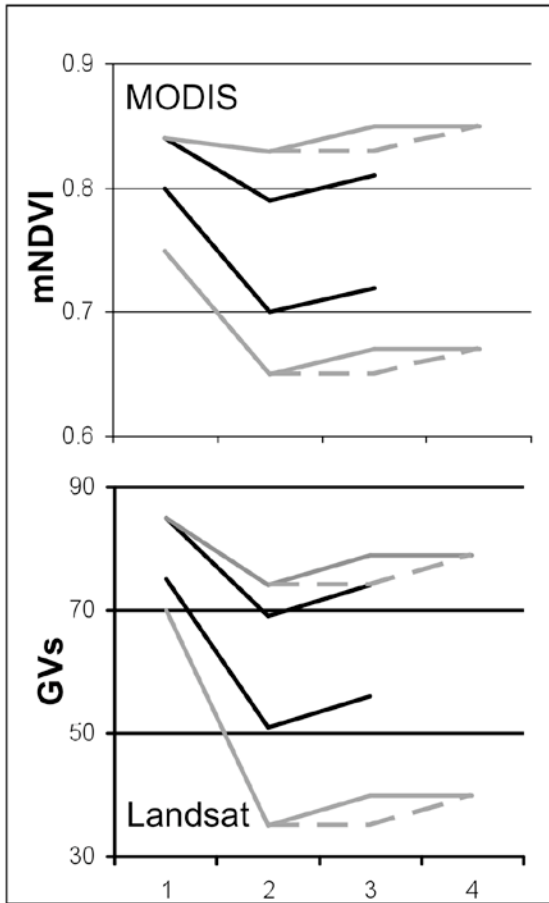
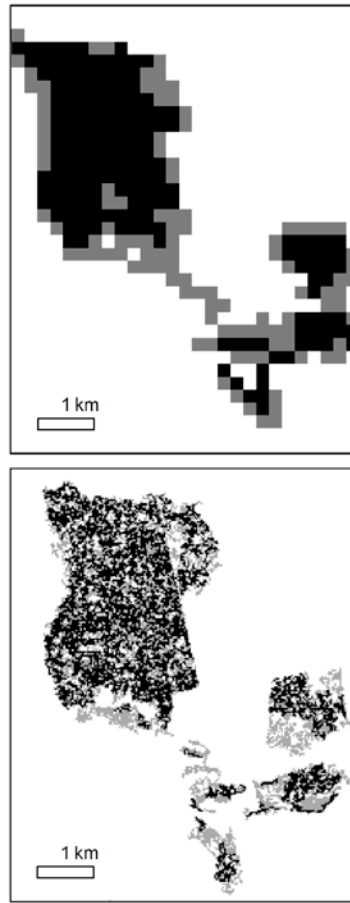


Figure 3: Time series of annual mean  $\pm$  1 S.D. MODIS mean dry-season NDVI (mNDVI, top left) and Landsat shade-normalized green vegetation fraction (GVs, bottom left) for calibration data on intact, logged, and burned forest and deforestation for pasture and cropland during 2002. Line plots show the mean trajectory for each class from MODIS (top right) and Landsat (bottom right). Table 1 lists the area and data source for each class. Table 2 provides the percent of each calibration data set that was classified as a core area by the BDR.

### 1. Trajectory Analysis



### 2. Contextual Analysis



### 3. Attribute Analysis

Metric	Landsat		MODIS	
	LC	HC	LC	HC
Size	-	>1.5 ha	-	>50 ha
Perimeter:Area	0.04-0.05	<0.04	-	-
Interior Fraction	-	-	0.5-0.6	>0.6
Mean Greenness	>62	<62	>0.8	0.71-0.8

Figure 4. The BDR algorithm has three main processing steps: 1) Trajectory Analysis: MODIS and Landsat time series trajectories are used to identify candidate core areas of canopy damage from fire (black) and growth regions (gray). Dashed lines show the range of values for 2-year recovery in growth regions. See Table 2 for pre-burn (1), drop, post-burn (2), and recovery (3,4) parameter ranges for each BDR trajectory. 2) Contextual Analysis: Large core areas (black) are joined to adjacent growth areas (gray) to generate forest burn scars. 3) Attribute Analysis: Individual burn scars are classified as low confidence (LC) or high confidence (HC) based on spatial and spectral metrics.

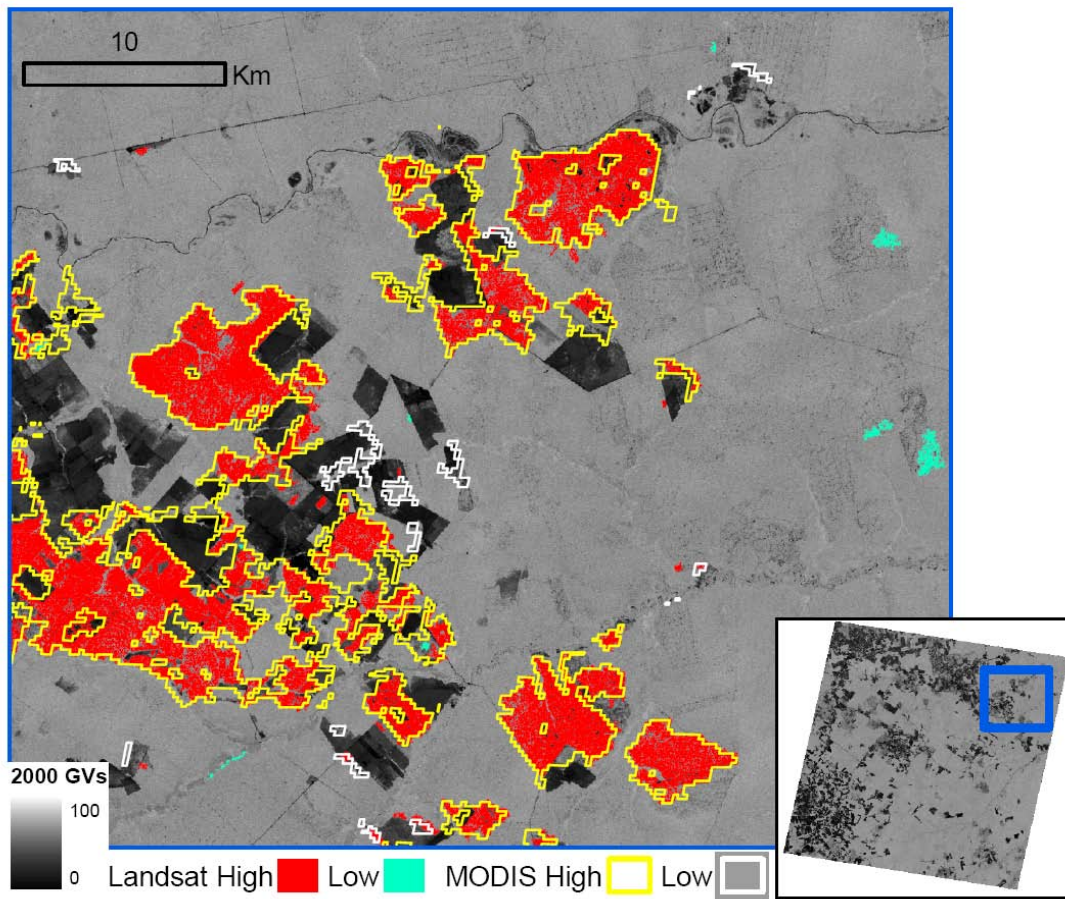


Figure 5. Landsat (solid colors) and MODIS (outlines) 1999 forest burn scar results classified according to high and low confidence based on spatial and spectral metrics for a subset of the study area (inset). The background image shows the shade-normalized green vegetation fraction (GVs) for 2000.

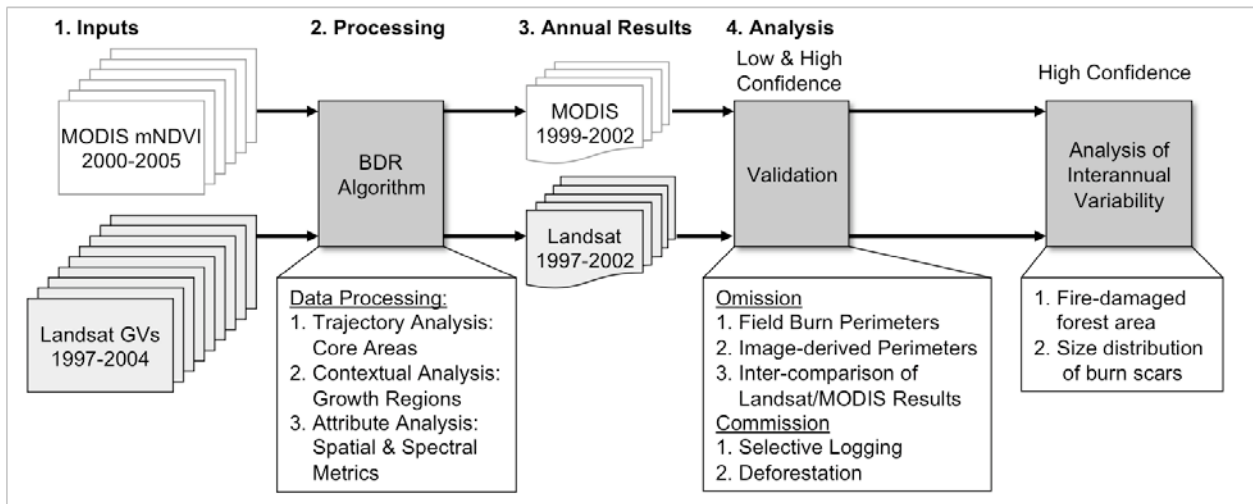


Figure 6. Flow diagram of data processing and analysis for annual maps of fire-damaged forest area from the BDR algorithm applied to time series of MODIS and Landsat data. The BDR algorithm identifies burned forest areas using a three-step process. All results from the BDR algorithm were compared to validation data on burned forest, selective logging, and deforestation, but only high-confidence burn scars were used to estimate interannual variability in burn scar size and total fire-damaged forest area.

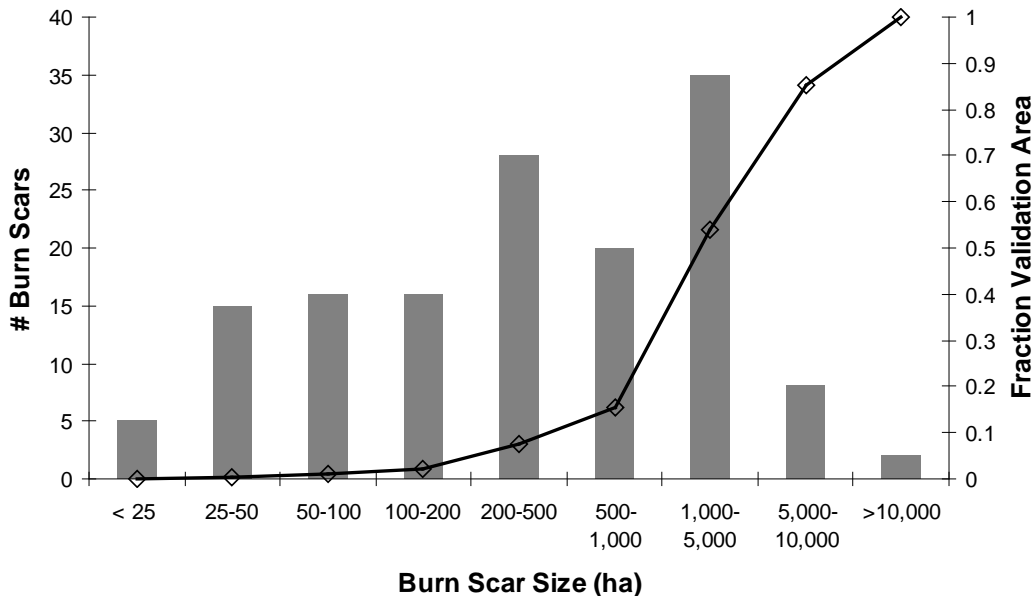


Figure 7. Number of burn scars (bars) and cumulative contribution to total validation fire-damaged forest area ( $\diamond$ ) by size class for 145 image-derived validation burn scars from 1999.

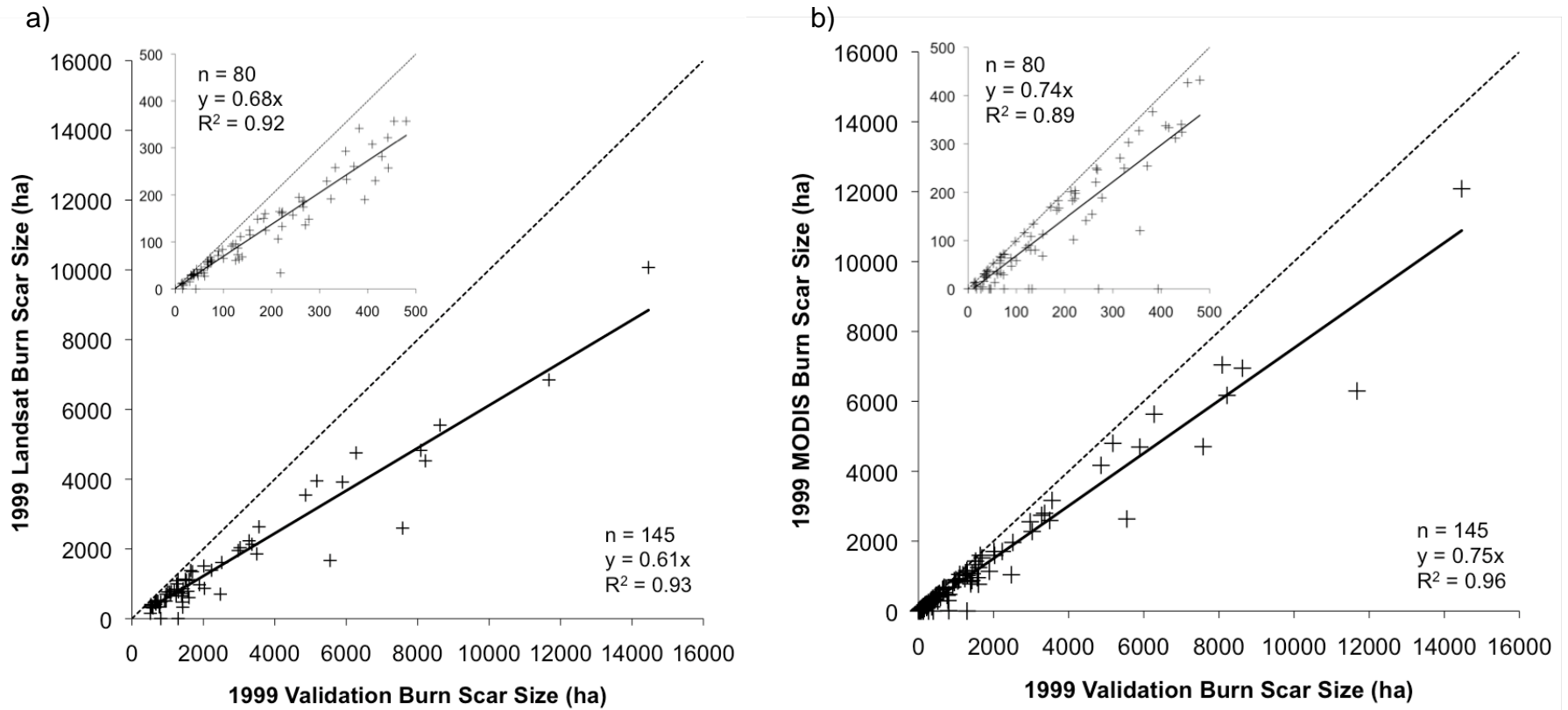


Figure 8. Validation of results from the BDR algorithm applied to time series of Landsat (a) and MODIS (b) data using 145 image-derived burn scars from 1999. The relationship between validation data and BDR results for burn scars <500 ha is shown in the upper left corner of each panel (inset). In each panel, a dashed 1:1 line is shown for reference.

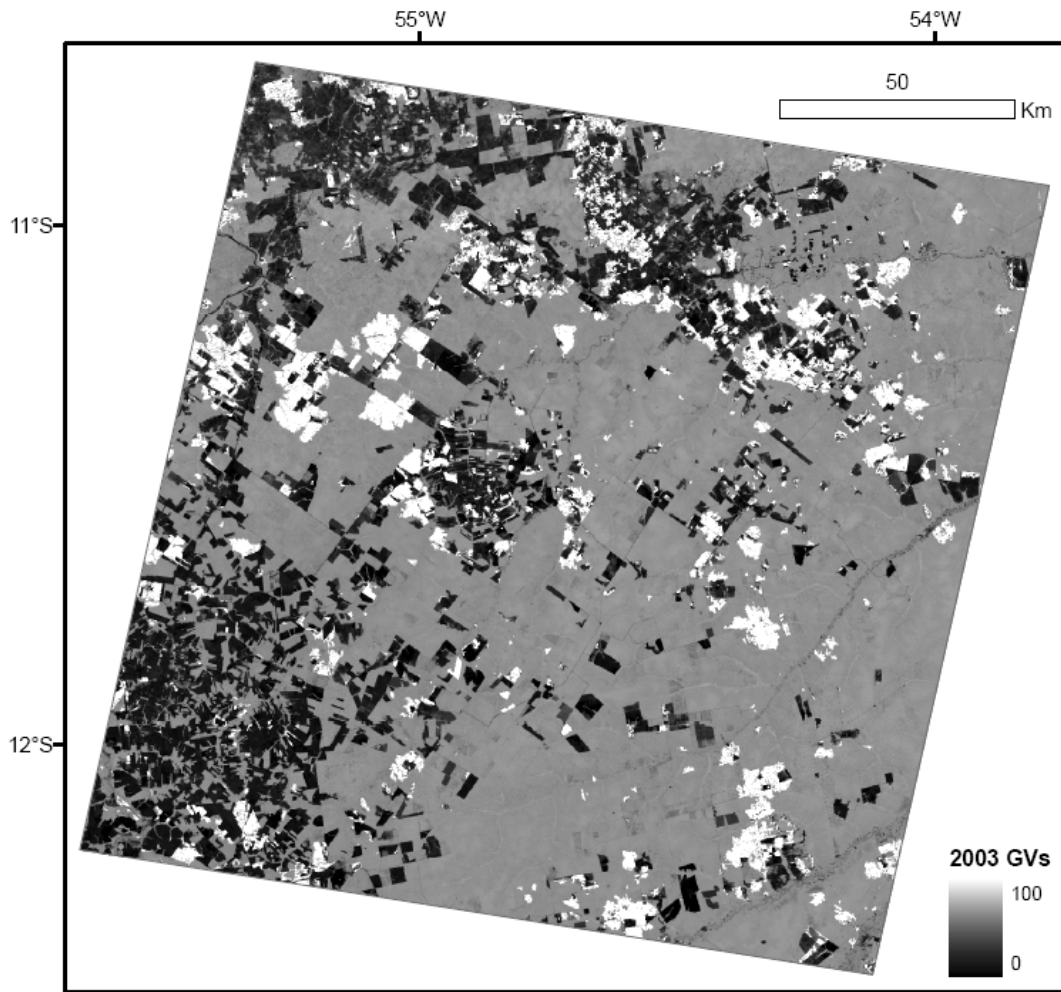


Figure 9. Total fire-damaged forest area during 1997-2002 (white) from the BDR algorithm applied to the time series of Landsat shade-normalized green vegetation fraction (GVs). Forested regions appear gray and deforested areas appear black in the background image of the study area from 2003.

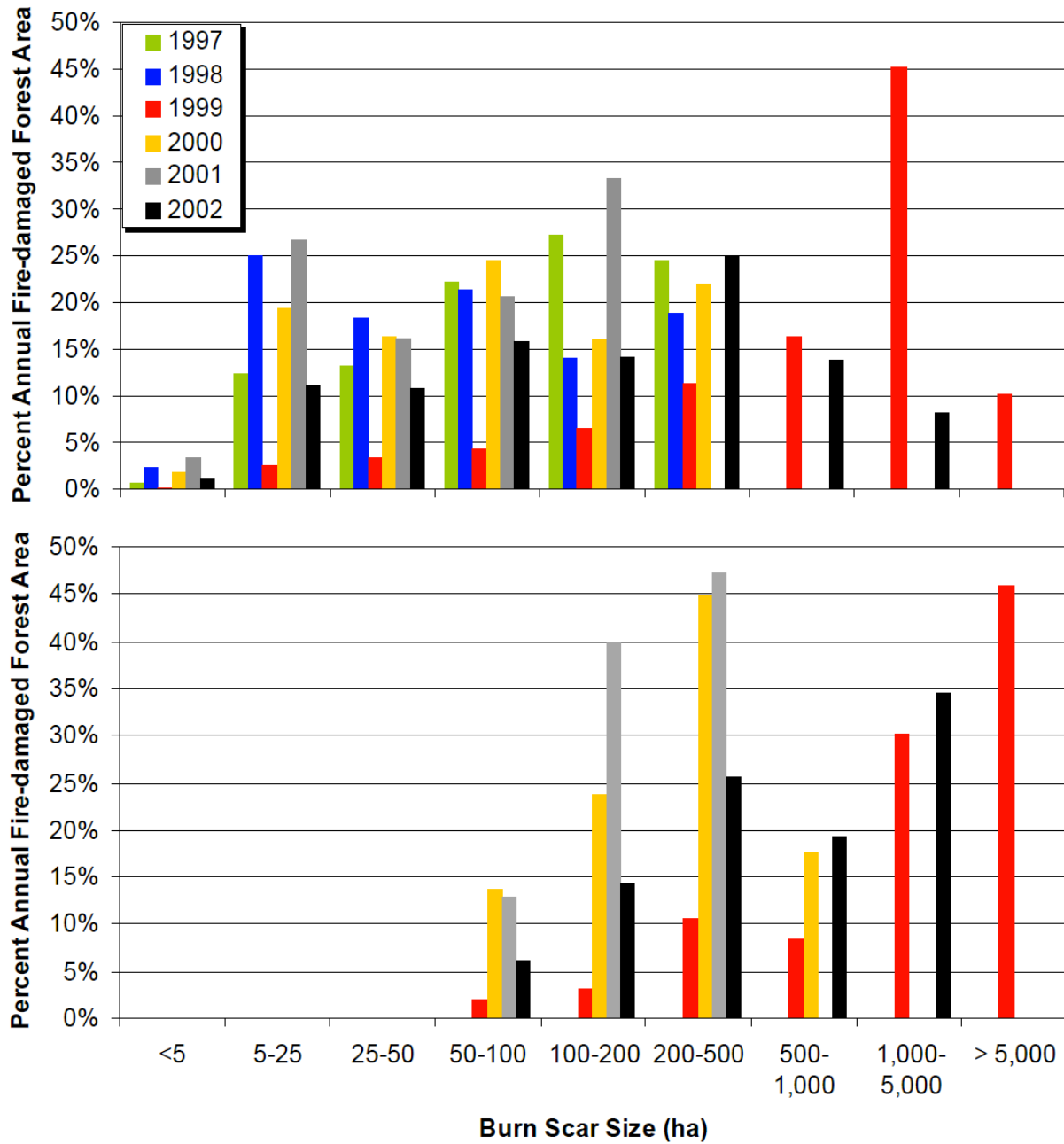


Figure 10. Percent contribution from burn scars of different sizes to annual high-confidence fire-damaged forest area for the BDR algorithm applied to time series of Landsat (top) and MODIS (bottom).

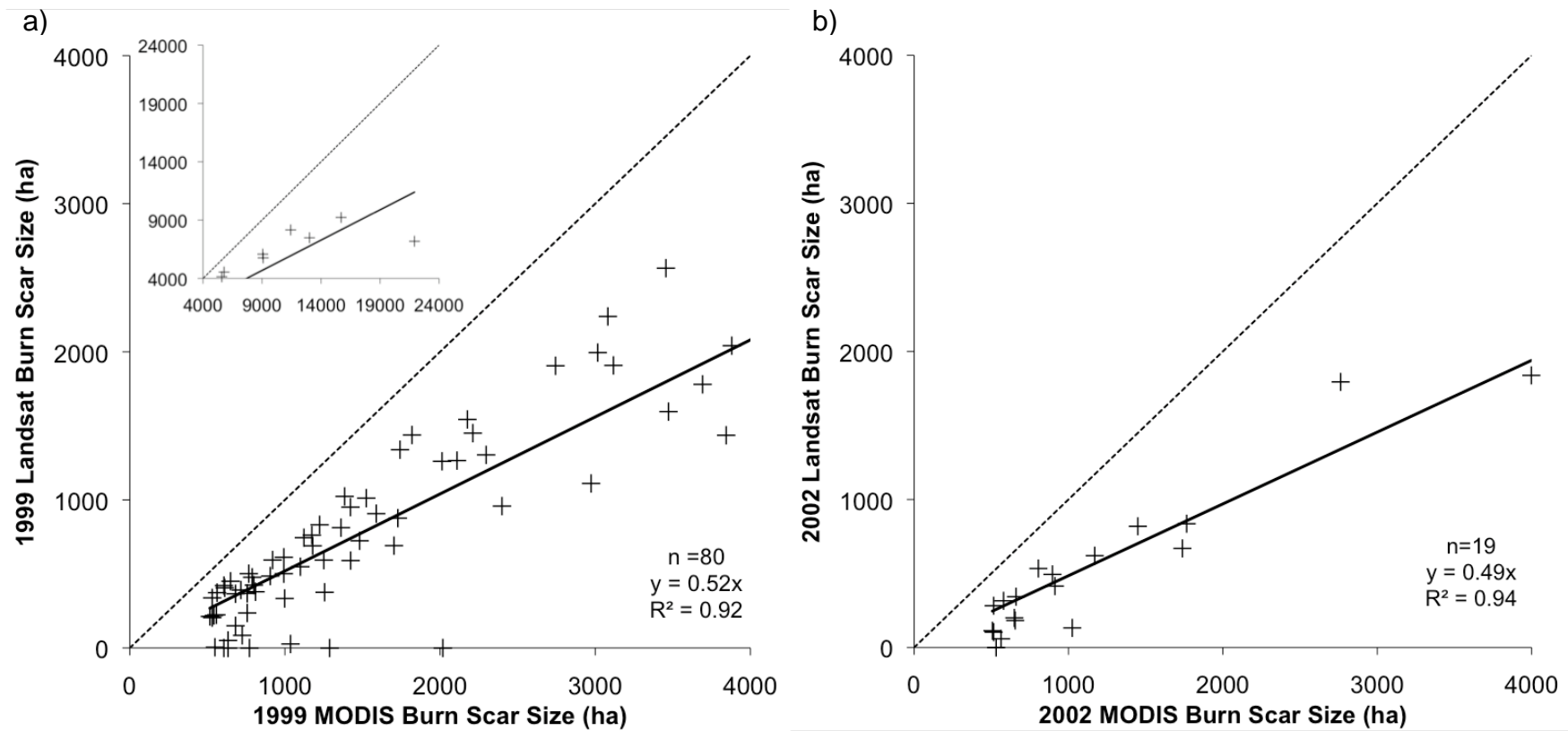


Figure 11. Estimated size of individual burn scars >500 ha in 1999 (a) and 2002 (b) from the BDR algorithm applied to time series of MODIS and Landsat data. For 1999, the relationship between MODIS and Landsat estimates of burn scar size for individual scars >4000 ha is shown in the upper left corner (inset). In each panel, a dashed 1:1 line is shown for reference.

